

Stellar populations of early-type galaxies in different environments

III. Line-strength gradients[★]

P. Sánchez-Blázquez^{1,2}, J. Gorgas², and N. Cardiel^{2,3}

¹ Laboratoire d'Astrophysique, École Polytechnique Fédérale de Lausanne (EPF L), Observatoire, 1290 Sauverny, Switzerland
e-mail: Patricia.SanchezBlazquez@epfl.ch

² Dpto. de Astrofísica, Fac. de Ciencias Físicas, Universidad Complutense de Madrid, 28040 Madrid, Spain

³ Calar Alto Observatory, CAHA, Apartado 511, 04004 Almería, Spain

Received 11 January 2006 / Accepted 19 April 2006

ABSTRACT

Aims. This is the third paper of a series devoted to the study of the stellar content of early-type galaxies. The goal of the series is to set constraints on the evolutionary status of these objects.

Methods. We present line-strength gradients for 22 spectral indices measured in a sample of 82 early-type galaxies in different environments, including the high-density cores of the Coma cluster, the Virgo cluster, poor groups, and isolated field galaxies. Using new evolutionary population synthesis models, we derive age and metallicity gradients, and compare the mean values with the predictions of different galaxy formation models. We explore the behaviour of individual chemical species by deriving the metallicity gradient with different indicators.

Results. We find that the strength of the metallicity gradient inferred from stellar population models depends on the specific Lick index employed. In particular, metallicity gradients obtained with CN₂ and C4668 combined with H β are steeper than those measured using Ca4227 or Fe4383. The correlation of the metallicity gradients with other parameters also depends on the specific index employed. If the metallicity gradient is obtained using CN₂ and Mgb, then it correlates with the central age of the galaxies. On the contrary, if Fe4383 or Ca4227 is used, the metallicity gradient correlates with the velocity dispersion gradient.

Conclusions. This may suggest that several mechanisms have helped to set the age and metallicity gradients in early-type galaxies. While we do not find any correlation between the metallicity gradient and the central velocity dispersion for galaxies in low-density environments, we find a marginal correlation between the metallicity gradient and the mass for galaxies in the centre of the Coma cluster. We also find a trend for which galaxies in denser environments show a steeper metallicity gradient than galaxies in less dense environments. We interpret these results in light of the different mechanisms proposed to explain the observed changes between galaxies as a function of environment.

Key words. Galaxy: abundances – galaxies: elliptical and lenticular, cD – galaxies: stellar content

1. Introduction

This is the third paper in a series devoted to studying the properties of the stellar populations in early-type galaxies as a function of their local environment. In Sánchez-Blázquez et al. (2006a, hereafter Paper I), we presented central Lick/IDS index measurements for a sample of 98 early-type galaxies and described their relation to the velocity dispersion. In Sánchez-Blázquez et al. (2006b, hereafter Paper II), we compared the indices with the stellar population synthesis models of Vazdekis et al. (2006, in preparation, hereafter V06) to derive ages and metallicities. These models are an improved version of those described by Vazdekis et al. (2003), strengthened by the addition of a new stellar library (Sánchez-Blázquez et al. 2006c). The synthetic spectra cover a spectral range of $\lambda\lambda 3500\text{--}7500\text{ \AA}$ at resolution 2.3 \AA . The previous papers concentrated on the analysis of the central regions of the galaxies. In this paper, we investigate the behaviour of these properties as a function of galactocentric radius.

It is well-known that early-type galaxies show a variation of their stellar population properties with radius. The first evidence of this phenomenon was observed in the colours of bulges and elliptical galaxies (see the review by Kormendy & Djorgovski 1989), and indicated that the central regions tend to be redder than the outer parts. Other authors have measured optical surface brightness profiles for large sets of local ellipticals (e.g., Franx et al. 1989; Peletier et al. 1990), reaching the same conclusion. The first study of gradients in the strength of absorption features was performed by McClure (1969). In a sample of 7 galaxies, McClure found that the C(41–42) index (a measure of the CN $\lambda\lambda 4216$ band strength) was stronger in the centres of the galaxies than at a distance of 1–1.5 kpc, which he interpreted to be the result of a metallicity difference between the two regions. Subsequent work in the field has explored the strength of absorption feature gradients using a broad range of line indices (Spinrad et al. 1971, 1972; Welch & Forrester 1972; Joly & Andriolat 1973; Oke & Schwarzschild 1975; Cohen 1979; Efstathiou & Gorgas 1985; Couture & Hardy 1988; Peletier 1989; Thomsen & Baum 1989; Gorgas et al. 1990; Boroson & Thompson 1991; Bender & Surma 1992; Davidge 1992; Davies et al. 1993; Carollo et al. 1993; González 1993;

[★] Full Table 1 and Table 2 are only available in electronic form at <http://www.edpsciences.org>

Fisher et al. 1995; Gorgas et al. 1997; Cardiel et al. 1998a; Mehlert et al. 2003). In general, these studies indicate the existence of intense gradients in CN λ 3883 and CN λ 4216, less pronounced gradients in the Mg λ 5176, G band, NaD, Ca H&K features, and in some lines of Fe I, and a weak or null gradient in H β , MgH, TiO, Ca I, and in the calcium triplet in the near-infrared. Most of these studies have suggested that the existence of gradients in the metallic spectral features is a consequence of a decreasing metallicity with increasing galactocentric radius (e.g., McClure 1969; Cohen 1979; Davies et al. 1993; Kobayashi & Arimoto 1999; Mehlert et al. 2003). Some, however, have argued that, apart from a variation of metallicity with radius, there is also a radial variation in the luminosity-weighted mean age of the stellar populations, with the central regions being younger than the outer regions (Gorgas et al. 1990; Munn 1992; González 1993; González & Gorgas 1996).

How the physical properties of galaxies vary with radius can prove invaluable for constraining the processes of galaxy formation and evolution. For example, metallicity gradients are a measure of the quantity, velocity, and duration of gas dissipation. Likewise, age and metallicity gradients contain information concerning the relative importance of interactions during galaxy formation.

In the classical models of monolithic collapse (Eggen et al. 1962; Larson 1974a; Carlberg 1984; Arimoto & Yoshii 1987; Gibson 1997), stars form in essentially all regions during the collapse and remain in their orbits with little inward migration, whereas the gas dissipates inwards, being continuously enriched by the evolving stars. In this way, the stars formed at the centres of galaxies are predicted to be more metal-rich than those born in the outer regions. Supernova-driven galactic winds (Mathews & Baker 1971; Larson 1974b; Arimoto & Yoshii 1987; Gibson 1997), initiated when the energy injected into the interstellar medium (ISM) by supernovae matches that of its binding energy, act to evacuate the galaxy of gas, thereby eliminating the fuel necessary for star formation. The external parts of the galaxy (with a shallower potential well) develop winds before the central regions, where the star formation and, therefore, the chemical enrichment continue for longer. The monolithic collapse models, therefore, predict very steep metallicity gradients as both processes – the dissipation of gas toward the central parts of the galaxy and the different timescales for the occurrence of the galactic winds – act in the direction of steepening any nascent metallicity gradient¹.

Simulations of galaxy mergers within the concordant hierarchical clustering cold dark matter framework (e.g., Cole et al. 1994; Baugh et al. 1996; Kauffmann 1996; Kauffmann & Charlot 1998) offer somewhat contradictory predictions as to the radial variation of stellar properties in early-type galaxies – while some (e.g., White 1980; Bekki & Shioya 1999) suggest that mergers lead of a flattening of metallicity gradients, others (e.g., van Albada 1982) argue that the gradients are affected only moderately by the mergers, as the violent relaxation preserves the position of the stars in the local potential. This apparent dichotomy between the simulations is driven in part by the sensitivity of the outcome to the fraction of gaseous versus stellar mass present in the progenitor galaxies. Broadly speaking, the predicted gradients are steeper if the progenitor galaxies have a large fraction of their pre-merger baryonic mass in the

form of gas. Furthermore, numerical simulations suggest that during the merger, a significant fraction of this gas migrates inward toward the central regions of the merging galaxies, resulting in increased central star formation (Barnes & Hernquist 1991). Mihos & Hernquist (1994) showed that the observed gradients in elliptical galaxies may be a consequence of the occurrence of secondary bursts of star formation triggered by these mergers.

One of the means to understanding the physical processes governing galaxy formation and evolution is to study the relations between gradients and other fundamental (global) properties of galaxies. For instance, dissipational collapse models predict a strong positive correlation between metallicity gradient and galactic mass. The empirical evidence for such putative correlations remains contentious – e.g., Gorgas et al. (1990, hereafter G90) did not find any relation between the Mg₂ gradient and the rotation or total luminosity of a sample of early-type galaxies, although they found some evidence of a positive correlation between the Mg₂ gradient and the central velocity dispersion (a probability of 95% in a non-parametric Spearman test). Conversely, Franx & Illingworth (1990) found a correlation between the colour gradient and local escape velocity (later confirmed by other authors, such as Davies et al. 1993), arguing that the aforementioned galactic winds were the dominant mechanism controlling the metal content of early-type galaxies. Davidge (1992) analysed 12 bright ellipticals, searching for correlations between the Mg₂ gradients and the central velocity dispersion (σ_0), the total luminosity, the shape of the isophotes, the fine structure parameter (Schweizer et al. 1990), and the anisotropy parameter (v/σ)*, which defines the degree of rotation in a galaxy (Binney 1978). Davidge found weak correlations between the Mg₂ gradient, (v/σ)* and σ_0 , and an absence of correlation with any of the other parameters. Carollo et al. (1993) carried out an exhaustive study of the gradients of several spectral features (Mg₁, Mg₂, NaD, TiO₁, TiO₂, and Fe5270) in a sample of 42 galaxies. Carollo et al. found a tendency for the slope of the gradients in the Mg₂ index to increase with the mass of the galaxy, but only for galaxies with masses below $10^{11} M_\odot$. Carollo & Danziger (1994) studied the line-strength gradients in Mg₂ and $\langle\text{Fe}\rangle$ for five early-type galaxies, confirming the dependency between metallicity and local potential well depth as a function of galactocentric radius, albeit with significant scatter. González & Gorgas (1996) surveyed the Mg₂ gradient literature available at the time, discovering that galaxies with steeper Mg₂ gradients also possess stronger central Mg₂. They proposed a scenario in which star formation episodes in the centre of the galaxies are responsible for the correlation, pointing out that its existence implies that the global mass-metallicity relation is flatter than the mass-metallicity relation inferred from the central values. Recently, Mehlert et al. (2003) found a correlation between the gradients of some spectral features and the velocity dispersion gradient (which can be considered a measure of the potential well depth gradient). In contrast with González & Gorgas, Mehlert et al. did not find a correlation between the line-strength index gradients and the central values, or between the index gradients and the central velocity dispersion.

The results to date are, to some extent, contradictory and therefore incapable of providing unequivocal support to any particular galaxy formation scenario. This contradictory nature is driven, in part, by the requisite high signal-to-noise data and associated care in data reduction necessary to extract reliable gradients. Further, very few absorption features (mainly Mg₂) have been systematically explored with a suitably large sample of ellipticals. Our work has been designed specifically to address

¹ Galactic winds *can* produce metallicity gradients without invoking dissipation (e.g., Franx & Illingworth 1990; Martinelli et al. 1998), with the local metallicity coupled directly to the local potential well depth and essentially independent of the galaxy formation collapse physics.

these shortcomings which have plagued the interpretation of the extant data, using a sample of 82 galaxies populating a range of local environmental conditions.

In Sect. 2, we describe the measurement of the line-strength gradients within our dataset. In Sect. 3, we compare these gradients with synthesis models to derive explicit age and metallicity gradients. Sections 4 to 7 analyse the stellar population gradients for a sample drawn from low density environments. In particular, Sect. 4 discusses the mean age and metallicity gradients, while in Sect. 5 we explore the existence of possible variations of the chemical abundance ratios with radius. In Sect. 6, we explore the existence of putative correlations between metallicity gradient and other galactic parameters. In Sect. 7, we use the stellar population global parameters, derived with the help of the gradients, to study whether the trends found in Papers I and II hold only for the central parts, or can be extended to the entire galaxy. Section 8 studies the mean gradients in the sample of galaxies drawn from the high-density core of the Coma cluster. Finally, in Sect. 9, we summarise our findings and conclusions.

2. Measurement of gradients

The parent sample from which galaxies are drawn consists of 98 early-type systems, of which 37 belong to the Coma cluster (high-density environment galaxies, hereafter HDEGs), while the rest are drawn from the field, small groups, and the Virgo cluster (low-density environment galaxies, hereafter LDEGs). Details of the sample, the observations, and associated data reduction, can be found in Paper I. From each fully reduced galaxy frame, a final frame was created by extracting spectra along the slit, binning in the spatial direction to guarantee a minimum signal-to-noise ratio per Å (S/N) of 20 in the spectral region of the H β index, ensuring a maximum relative error for this index (assuming a typical value of 1.5 Å) of 20% (see Cardiel et al. 1998b). Those galaxies that did not have a minimum of 4 spectra along the radius meeting this criterion were eliminated from the final sample, which left a total of 82 galaxies of sufficient quality to measure gradients – 21 HDEGs and 61 LDEGs.

An equivalent radius $\bar{r}(i)$ was assigned to each binned spectrum:

$$\bar{r}(i) = \frac{\int_i \mu_i(r) r dr}{\int_i \mu_i(r) dr}, \quad (1)$$

where

$$\mu_i(r) = k 10^{b_i r}. \quad (2)$$

The value of b_i for each spectrum was calculated by fitting the number of counts in each row of the detector (including all the rows in each spectrum, plus the neighbours) to the relation

$$\log N = b_i r + c, \quad (3)$$

where N is the number of counts, r the radius in arcseconds, and c a constant. We projected the gradients over the major axis, multiplying the mean radius by a factor

$f = \sqrt{\cos^2 \theta + (\frac{a}{b} \sin^2 \theta)}$, where θ is the difference between the major axis and the position angle of the slit, and a and b represent the major and minor axis of the galaxy, respectively. The a , b , and θ values for each galaxy can be found in Table 2 of Paper I.

Radial velocities and velocity dispersions were measured for each spectrum as a function of galactocentric radius, as described in Paper I. The rotation curve and the velocity dispersion profile were used to measure the Lick/IDS indices at the resolution defined by this system and to correct them for velocity broadening (again, as described in Paper I). Instead of using the individual values of the velocity dispersion for each spectrum measured at each radial “bin”, we fitted a smooth curve to the σ profile. This minimises the errors in the derived velocity dispersion, due to the lower signal-to-noise ratios in the external parts of the galaxies. Residual [OIII] emission profiles were also estimated as described in Paper I. These values were used to correct the H β index for emission, using the relation derived by Trager et al. (2000a) – $\Delta H\beta = 0.6 [\text{OIII}]$, where $\Delta H\beta$ is the correction to the index and [OIII] the equivalent width of the [OIII] λ 5007 emission line. The Mgb and Fe5015 indices were also corrected from emission, as was done in the central spectra. The final kinematic, line-strength and emission profiles, together with their associated errors, are presented in Sánchez-Blázquez (2004).

We measured 19 Lick/IDS indices defined by Trager et al. (1998) for all the galaxies except for those observed in Run 3, for which only 15 indices could be measured. With the aim of reducing the random errors in the external parts of the galaxies, we have defined the following composite indices:

$$HA = \frac{H\gamma_A + H\delta_A}{2} \quad (4)$$

$$\text{Balmer} = \frac{H\gamma_A + H\delta_A + H\beta}{3}. \quad (5)$$

To obtain the final values for the line strength indices, we applied the same corrections as for the central indices (see Paper I). Finally, all indices were transformed into magnitudes, as described in Paper I.

Although the behaviour of the indices as a function of galactocentric radius is not perfectly linear for all 82 galaxies, with the aim of obtaining a quantitative measurement of their values, we performed a linear fit, weighted by the errors over all the indices, to the relation $I' = c + d \log \frac{r}{a_e}$, where I' represents the index expressed in magnitudes, a_e is the effective radius projected over the major axis, i.e., $a_e = r_{\text{eff}} / \sqrt{\frac{a}{b}}$ (r_{eff} being the effective radius), and d the index gradient, hereafter denoted by $grad$. This projection can be done under the assumption that the contours of constant I' coincide with the isophotes, which has been confirmed by several earlier studies (e.g., Davies et al. 1993). To avoid the uncertainties and radial flattening due to seeing effects, the data within the central area corresponding to the seeing were excluded from the fit. The seeing was estimated directly from the observations on the 4 different runs. Figure 1 shows some examples of the line-strength gradients for the galaxy NGC 2832.

To check the assumption of linearity for the gradients, we have compared the central values derived in Paper I (integrated within an equivalent aperture of 4'' at redshift $z = 0.016$ – i.e., ~ 1.3 kpc), with the expected values for this aperture inferred from the gradients. Figure 2 shows this comparison for all the indices. Within each panel, the mean offset (Δ) and the root mean square of the deviations (σ) are indicated. In general, the agreement is very good – the offsets are not statistically significant for any of the indices, and the scatter is compatible with the errors, lending support to the adopted approximation of a linear fit.

Table 1, available in the electronic edition and online², lists the gradients in all the line-strength indices measured for each

² <http://www.ucm.es/info/Astrof/users/pat/pat.html>

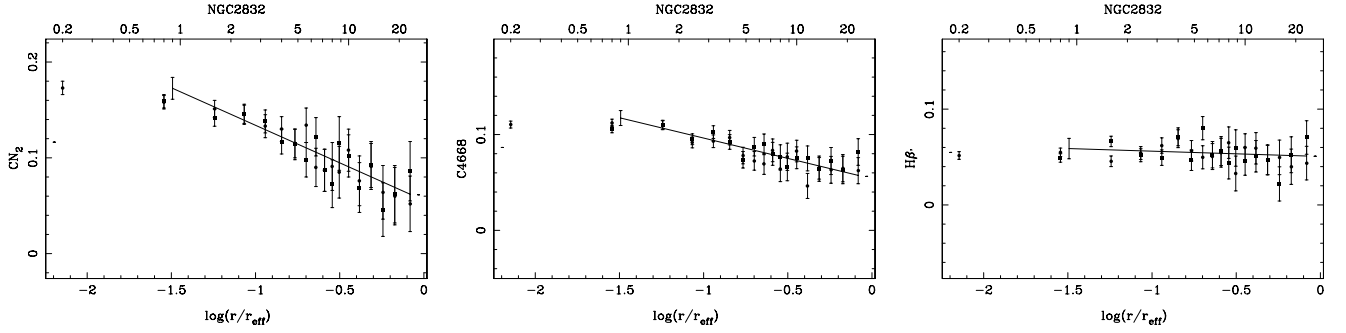


Fig. 1. Variation of the indices CN_2 , C4668 , and $\text{H}\beta$ as a function of galactocentric radius for the galaxy NGC 2832. The upper axes show the radial distance from the centre of the galaxy in arcseconds. The solid line represents a linear fit to the data, as described in the text. The data within $0''.9$ of the galaxy's centre were excluded from the fit to minimise the effects of seeing on the fitted gradients.

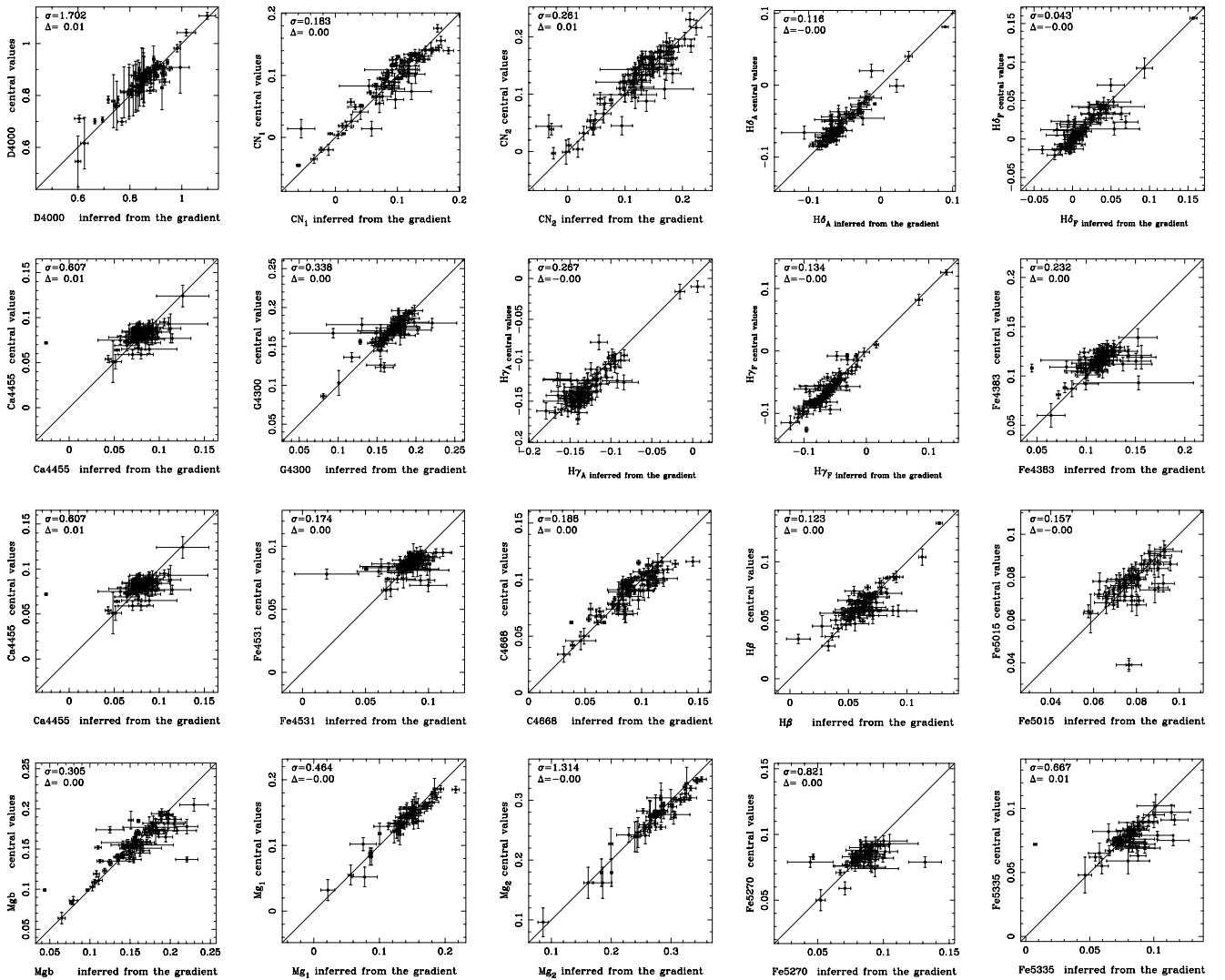


Fig. 2. Comparison of the Lick indices measured in the central spectra (integrated within an equivalent aperture of $4''$ at redshift $z = 0.016$ – i.e., ~ 1.3 kpc) and the indices obtained from the gradients integrating over the same aperture; σ indicates the root mean square and Δ the mean offset between both measurements. The solid line indicates the 1:1 correspondence. In all cases, the mean offsets are not statistically significant.

of the 82 galaxies in our sample. A portion of this table is reproduced here to demonstrate its content and structure.

3. Gradients in age and metallicity

Figure 3 shows the line-strength gradients in Fe4383 , Mgb , and $\text{H}\beta$, presented in index-index diagrams that combine both

the central values and the line-strengths at one effective radius. Each central measurement is connected to its corresponding measurement in the outer region. The stellar population models of V06 are overplotted. As can be seen, most of the lines tend to be nearly parallel (although, admittedly, not entirely) to the iso-age lines taken from the theoretical grid, which indicates that the gradients are mostly due to variations in metallicity. However,

Table 1. Velocity dispersion and line-strength gradients for the sample of 82 galaxies. A portion of the table is shown for guidance regarding its form and content. For each galaxy and index, the first line shows the measured gradient, while the second row lists its corresponding formal error. The full table is available in electronic form at <http://www.edpsciences.org>.

Galaxy	σ	D4000	H δ_A	H δ_F	CN ₂	Ca4227	G4300	H γ_A	H γ_F	Fe4383
NGC 221	-0.0877	-0.0520	-0.0014	0.0008	-0.0247	-0.0110	0.0104	0.0018	0.0079	0.0025
	0.0126	0.0058	0.0023	0.0026	0.0057	0.0035	0.0025	0.0020	0.0032	0.0017
	Ca4455	Fe4531	C4668	H β	Fe5015	Mg ₁	Mg ₂	Mgb	Fe5270	Fe5335
	0.0027	-0.0030	-0.0037	-0.0021	0.0052	-0.0007	0.0092	-0.0017	-0.0038	0.0020
	0.0019	0.0016	0.0017	0.0016	0.0019	0.0011	0.0022	0.0018	0.0011	0.0017

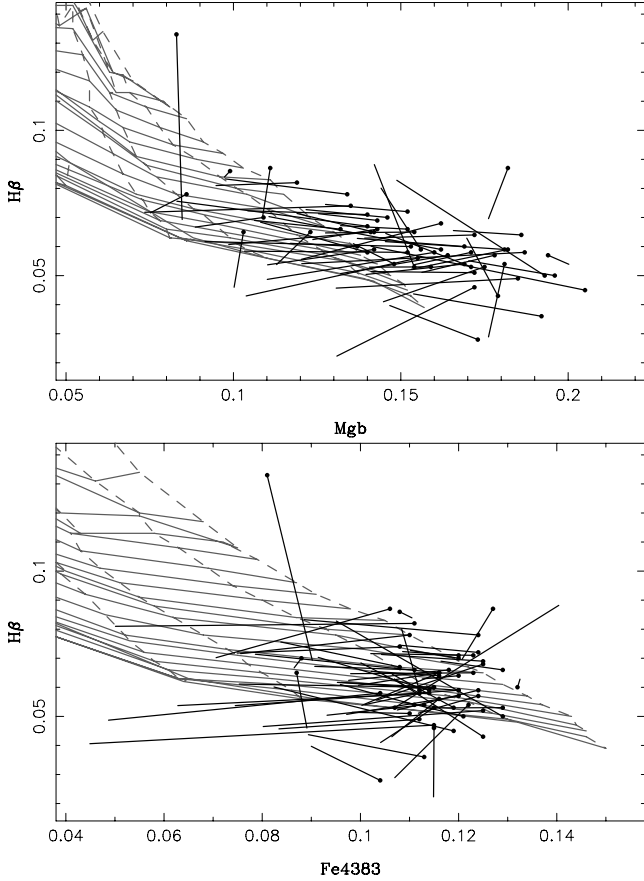


Fig. 3. Index-index diagrams using the models of V06. Solid lines represent the predictions for populations of constant age (*top to bottom*, 1.41, 2.00, 2.82, 3.98, 5.62, 7.98, 11.22, 15.85 Gyr), while dashed lines show populations of constant metallicity (*left to right*, $[M/H] = -0.68, -0.38, 0.0, +0.2$). The solid circles in the figure indicate the position of the centre of the galaxies, while the lines connect with the measurements at one effective radius.

there are several galaxies that show significant variations in both age and metallicity with radius. We return to this point towards the end of this section.

To quantify this behaviour, we have transformed the line-strength gradients into age and metallicity gradients using the model predictions of V06, who make use of the code of Vazdekis (1999) updated with a new and improved stellar library (MILES, Sánchez-Blázquez et al. 2006c; these models will be presented in the forthcoming paper V06).

With the aim of minimising the effects of low signal-to-noise data, we designed a method that makes simultaneous use of 10 different indices. The selected indices are: H δ_A , CN₂,

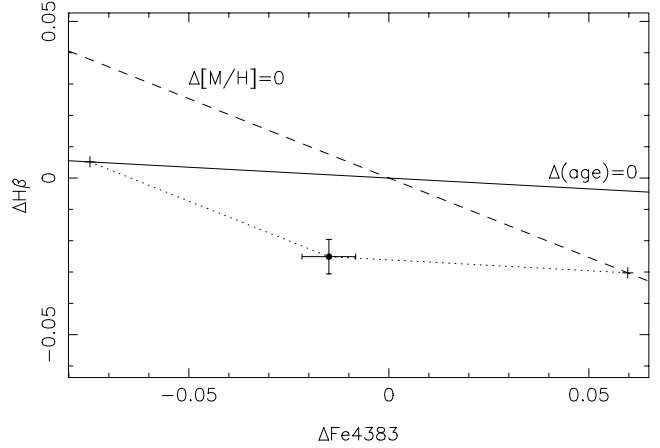


Fig. 4. Variations in the H β and Fe4383 line-strength indices expected through changes in metallicity at a constant age of 10 Gyr (solid line) and due to variations in the age at constant solar metallicity (dashed line). The point represents the values of the gradients for the galaxy NGC 4842A with their associated error bars. The dotted lines indicate the projections of the values over the lines of constant age and constant metallicity.

Ca4227, G4300, H γ_A , Fe4383, H β , Fe5015, H α , and Balmer. We checked that the results did not depend on the particular choice of indices. None of the Mg indices were employed, as they could not have been measured in all the galaxies from Run 3, due to the wavelength coverage of the spectra. To derive single estimates of age and metallicity gradients, we followed a procedure that is divided into two steps: (i) obtaining individual errors for the age and metallicity gradients for all the galaxies in each index-index diagram; and (ii) deriving the final values of the age and metallicity gradients, along with their associated errors.

3.1. Obtaining the errors in the age and metallicity gradients

We first calculated the slopes of the constant age and metallicity lines in the models. The slopes of these lines change with the absolute values of age and metallicity but, in the region in which the galaxies are located, the values are almost constant. The derived slopes define a new diagram that we call “ Δ index– Δ index” – in the associated Fig. 4, the dashed line represents the expected gradients in the indices if these were due, exclusively, to a variation in age (assuming a constant solar metallicity). On the other hand, the solid lines show the predicted gradients if the only parameter changing with radius was the metallicity (assuming a constant age of 10 Gyr). Figure 4 also shows the gradients in H β and Fe4383 measured in the galaxy NGC 4842A. To derive the age and metallicity gradients,

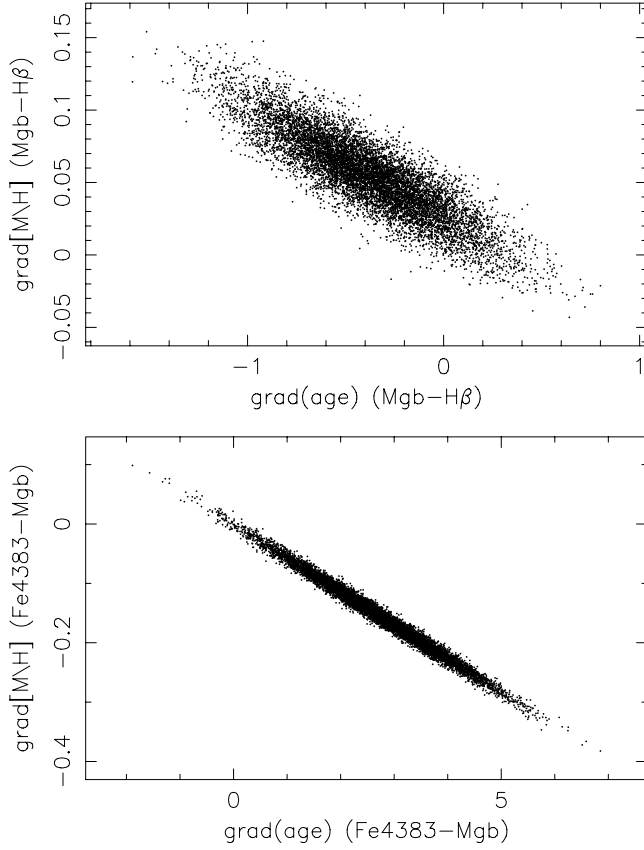


Fig. 5. Age and metallicity gradients obtained for the 10^4 Monte Carlo simulations performed in the diagrams $\Delta H\beta$ – ΔMgb (top panel) and ΔMgb – $\Delta Fe4383$ (bottom panel) for NGC 4842A. The correlation of the errors is larger when the age and metallicity are inferred from the latter.

we project the position of the galaxy over the lines $\Delta \text{age} = 0$ and $\Delta [M/H] = 0$, and interpolate the projection over these lines.

For each galaxy, and in every Δindex – Δindex diagram, we performed 10^4 Monte Carlo simulations in which each point was perturbed with our errors, following a Gaussian probability distribution. For each simulation, an age and metallicity gradient was obtained. This process was repeated with all possible paired combinations of indices. As an illustration, Fig. 5 shows the values of age and metallicity gradients derived for NGC 4842A, using the $\Delta H\beta$ – ΔMgb and ΔMgb – $\Delta Fe4383$ diagrams. As can be seen, due to the non-orthogonality of the index-index diagrams, there is an artificial anti-correlation between the age and the metallicity gradients. To obtain the error in the age and metallicity gradient for each galaxy, in every diagram, we projected these ellipses over the x - and y -axes and calculated the standard deviation of the resultant Gaussian. We denote the typical errors by $\sigma(\text{grad}[\text{age}])_i$ and $\sigma(\text{grad}[M/H])_i$, where i refers to each index-index diagram.

3.2. Obtaining the age and metallicity gradients

Once we have obtained the typical errors associated with the inferred age and metallicity gradients for each index-index combination, we again performed (for each galaxy) 10^4 Monte Carlo simulations, into which Gaussian noise was added to each line-strength index. Simulations were performed for each index independently, as opposed to each index-index diagram (note that once an index value is simulated, its particular value is fed

simultaneously to all the possible diagrams, taking into account the fact that not all of the different diagrams are independent).

We then measured the age and metallicity gradients of all the values obtained in all the simulations j , using all the different diagrams i . The mean age and metallicity gradient of simulation j was obtained as an average of the age and metallicity gradients obtained for this particular simulation, using all the different diagrams i , namely,

$$\text{grad}[\text{age}]_j = \frac{\sum_{i=1}^{n_{\text{com}}} \frac{\text{grad}[\text{age}]_{i,j}}{\sigma(\text{grad}[\text{age}])_i^2}}{\sum_{i=1}^{n_{\text{com}}} \frac{1}{\sigma(\text{grad}[\text{age}])_i^2}}, \quad (6)$$

and

$$\text{grad}[M/H]_j = \frac{\sum_{i=1}^{n_{\text{com}}} \frac{\text{grad}[M/H]_{i,j}}{\sigma(\text{grad}[M/H])_i^2}}{\sum_{i=1}^{n_{\text{com}}} \frac{1}{\sigma(\text{grad}[M/H])_i^2}}, \quad (7)$$

where $\text{grad}[\text{age}]_{i,j}$ represents the age gradient obtained with the i th diagram in the simulation j , $\sigma(\text{grad}[\text{age}])_i$ the uncertainty of the age gradient in the i th diagram (obtained in the first step of the process), $\text{grad}[M/H]_{i,j}$ the metallicity gradient in simulation j (using the i th diagram), and $\sigma(\text{grad}[M/H])_i$ the error in the metallicity gradient in this diagram; n_{com} indicates the total number of diagrams, which is the number of possible index pairs ($n_{\text{com}} = 45$).

Finally, the age and metallicity gradients for each galaxy were calculated as the mean values of all the simulations, i.e.,

$$\text{grad}[\text{age}]_{\text{final}} = \sum_{j=1}^{n_{\text{sim}}} \frac{\text{grad}[\text{age}]_j}{n_{\text{sim}}}, \quad (8)$$

and

$$\text{grad}[M/H]_{\text{final}} = \sum_{j=1}^{n_{\text{sim}}} \frac{\text{grad}[M/H]_j}{n_{\text{sim}}}, \quad (9)$$

where n_{sim} is the number of simulations performed for each line-strength index gradient. The final errors in the age and metallicity gradients were obtained as the standard deviations of the values obtained for each simulation, that is

$$\sigma_{(\text{age})} = \sqrt{\frac{\sum_{j=1}^{n_{\text{sim}}} (\text{grad}[\text{age}]_j - \text{grad}[\text{age}]_{\text{final}})^2}{n_{\text{sim}} - 1}}, \quad (10)$$

and

$$\sigma_{([M/H])} = \sqrt{\frac{\sum_{j=1}^{n_{\text{sim}}} (\text{grad}[M/H]_j - \text{grad}[M/H]_{\text{final}})^2}{n_{\text{sim}} - 1}}. \quad (11)$$

This process was performed for all 82 galaxies in our sample. The final values for the age and metallicity gradients obtained in this way, together with the associated errors, are listed in Table 2.

Figure 6 shows three different Δindex – Δindex diagrams in which we have overplotted the galaxies in low-density environments. The lines of constant age and metallicity divide these diagrams into four distinct regimes. These regimes indicate the

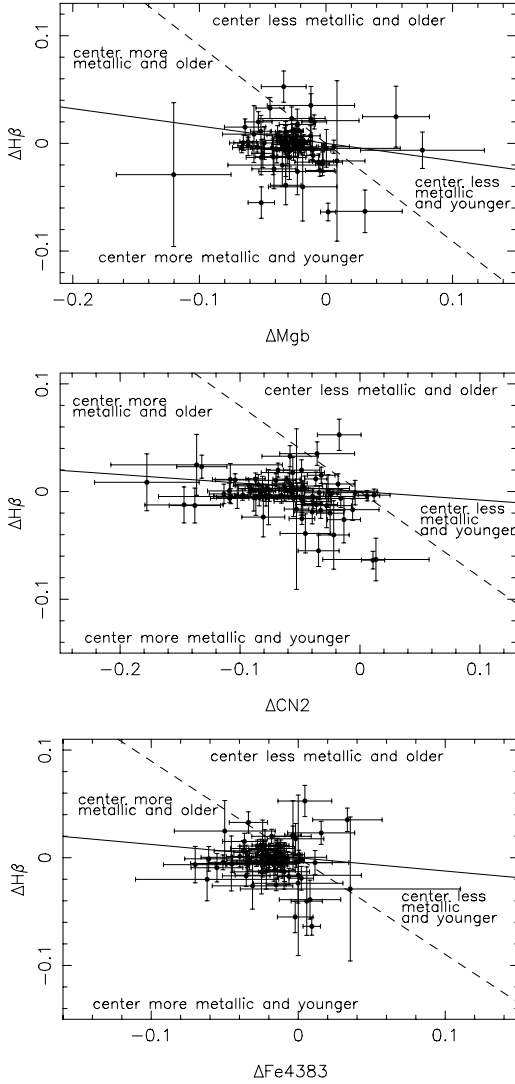


Fig. 6. Δ index– Δ index diagrams combining the $H\beta$ gradient with Mgb, CN_2 , and Fe4383. Solid lines indicate the slope of the predictions at constant age (10 Gyr); the dashed line shows the slope of the simple stellar population at solar metallicity. The solid circles represent the values of the line-strength gradients for the sample of galaxies in low-density environments.

position of the galaxies with positive/negative differences in age and metallicity between the central and the external parts, as is labeled in the panels. As can be seen, most of the galaxies are situated in the regime consistent with their centres being younger and more metal-rich than their outer regions. The bulk of the galaxies, however, are further away from the line $\Delta[M/H] = 0$ than from the line $\Delta\text{age} = 0$, suggesting that the gradients in the line-strength indices are due (mostly) to variations of metallicity with radius.

4. Mean gradients

The predicted mean values of the age and metallicity gradients are dependent upon the merging history of the galaxies. In general, dissipative processes tend to steepen the metallicity gradient, while major mergers are expected to dilute it. In the simulations of Kobayashi (2004), the typical gradients for non-merger and merger galaxies are $\Delta[Fe/H]/\Delta\log r \sim -0.45, -0.38$, $\Delta[O/H]/\Delta\log r \sim -0.25, -0.24$, and $\Delta\log Z/\log r \sim -0.30$,

-0.24 , respectively. We now analyse the mean age and metallicity gradients for the sample of LDEGs. Table 3 lists these values, together with relevant associated statistics (see below).

4.1. Age gradients

The mean age gradient for the sample of LDEGs is $\Delta\log(\text{age})/\log r = 0.082 \pm 0.015$. A t -test indicates that the probability of this value being different from zero by chance is $<0.1\%$. The positive gradient indicates that, on average, the centres of the galaxies are younger (or at least, they contain a percentage of younger stars, which make the mean luminosity-weighted age lower) than the outer parts. The existence of a significant age gradient is difficult to explain within monolithic collapse scenarios, as the timescales for star formation are necessarily very short, but it does suggest that secondary episodes of star formation have occurred recently in the centres of the galaxies.

Little work has been done to date on the derivation of age gradients within early-type galaxies. Indeed, most of the extant studies of gradients in the literature *assume* the absence of an age gradient in order to derive the metallicity gradient. Munn (1992) was the first author who studied, in a systematic way, the variation of age with the galactocentric radius. From a sample of seven early-type galaxies, Munn combined the $CN\lambda 3883$ and $CN\lambda 4216$ features with the D4000 index to compare them with the prediction of stellar population models. Since the age calibration employed by Munn was necessarily restricted to the assumption of solar metallicity, his ability to quantify the inferred gradients was limited. He did, however, conclude that to explain the dispersion and trends in the CN –D4000 diagrams, a variation of at least two parameters with radius was necessary (as suggested already by G90), with age and metallicity being the obvious candidates. Using the stellar population models of Worthey (1994), González (1993) found a mean variation in the age of his sample of galaxies of $\sim 20\%$ from the centre to the effective radius (he also found a variation of $\sim 50\%$ in metallicity). Fisher et al. (1996) found that the centres were slightly younger than the external parts in their sample of lenticulars, although they did not quantify the result. Contrary to these results, Mehlert et al. (2003) found a mean age gradient compatible with being null in a sample of galaxies. The discrepancy between the above results and those of Mehlert et al. (2003) *may* be due to the different environments from which the samples were drawn. We analyse the gradients for the HDEGs in Sect. 8.

Table 3 also shows the values of the rms dispersion about the mean value (σ) and the scatter expected from the errors (σ_{exp}). We performed a χ^2 test to compare these values, and the results are shown in the 8th column of the table. There is a real scatter in the age gradients between galaxies that cannot be explained by the errors, which is consistent with the earlier results of G90. We have explored possible correlations between the age gradients and other parameters of the galaxies, including (but not limited to) the central velocity dispersion, but we have not found any significant correlations.

4.2. Metallicity gradients

The mean metallicity gradient in our sample of LDEGs is $\Delta[M/H]/\Delta\log r = -0.206 \pm 0.019$. Earlier studies have derived comparable gradients using, primarily, $\langle Fe \rangle$ and Mg indices. For example, Couture & Hardy (1988), using the Mg_2 index, found a variation in metallicity with radius of $\Delta[M/H]/\log r = -0.25$.

Table 3. Mean gradients of age, [M/H], and metallicity, derived with different indices for LDEGs. σ : typical deviation; N : number of galaxies; N_{eff} : effective number of points, $N_{\text{eff}} = \left[\sum (1/\sigma^2) \right]^2 / \sum (1/\sigma^2)$; t : t -statistic to check the hypothesis “mean $\neq 0$ ”; σ_{exp} : typical deviation expected from errors; α : level of significance to reject the hypothesis “ $\sigma = \sigma_{\text{exp}}$ ”. The last column contains the t -statistic used to test the hypothesis “mean $\text{grad}[\text{M}/\text{H}] = \text{mean grad}[\text{M}/\text{H}]$ ” (with different indices).

	Mean	σ	N	N_{eff}	t	σ_{exp}	α	t
grad (log age)	0.082 ± 0.015	0.117	61	19.62	3.1	0.032	1.63E-13	
grad [M/H]	-0.206 ± 0.019	0.151	61	17.25	5.7	0.075	4.3E-22	
grad [M/H] (CN ₂ -H β)	-0.582 ± 0.032	0.249	61	23.14	11.2	0.111	2.6E-31	5.94
grad [M/H] (C4668-H β)	-0.459 ± 0.028	0.219	61	21.78	9.8	0.078	0.000	4.26
grad [M/H] (Fe4383-H β)	-0.197 ± 0.025	0.197	61	15.31	3.9	0.109	1.2E-14	0.14
grad [M/H] (Mgb-H β)	-0.407 ± 0.039	0.302	61	14.53	5.1	0.138	5.3E-31	2.30
grad [M/H] (Ca4227-H β)	-0.238 ± 0.034	0.269	61	19.18	3.4	0.178	2.9E-7	0.45

G90 measured mean gradients in their sample of early-type galaxies of $\Delta[\text{M}/\text{H}]/\log r = -0.23 \pm 0.09$ and $\Delta[\text{M}/\text{H}]/\log r = -0.22 \pm 0.10$, using the Mg₂ and $\langle\text{Fe}\rangle$ indices, respectively (later confirmed by Davies et al. 1993). To transform the line-strength gradients into metallicity gradients, each of these studies used the Mould (1978), Burstein (1979), and Faber et al. (1985) calibrations. In all these cases, they assumed a null age gradient. Fisher et al. (1995), through the comparison of the gradients of Mg₂, H β , and $\langle\text{Fe}\rangle$ with the stellar population models of Worthey (1994), obtained a metallicity gradient of $\Delta[\text{M}/\text{H}]/\log r = -0.25 \pm 0.1$. Finally, Mehlert et al. (2003), using the population synthesis models of Thomas et al. (2003), obtained a metallicity gradient of $\Delta[\text{M}/\text{H}]/\log r = -0.10 \pm 0.12$, significantly more shallow than previous studies had found. The values derived in the current study are consistent with the extant literature and suggest that early-type galaxies exhibit a reduction in metallicity of $\sim 40\%$ per decade of variation in radius. This value is considerably lower than the values predicted by the dissipative collapse models. For example, Larson’s hydrodynamical simulations gave $\Delta \log Z / \Delta \log r \sim -0.35$ (Larson 1974a,b) and -1.0 (Larson 1975), and Carlberg’s (1984) N -body simulations gave $\Delta \log Z / \Delta \log r \sim -0.5$. It should be stressed, though, that these particular models leave significant room for improvement, due to the absence of essential physical processes, including star formation, thermal feedback from supernovae, and chemical enrichment.

Finally, we compared the dispersion about the mean values ($\sigma = 0.151$) and the scatter expected from the errors ($\sigma_{\text{exp}} = 0.075$) by performing a χ^2 test. The hypothesis “ $\sigma_{\text{exp}} = \sigma$ ” can be rejected at a low significance level (see Col. 8 of Table 3). To investigate the causes of the variation in the metallicity gradients among galaxies, we explore putative correlations of the gradients with other physical galaxy parameters in Sect. 6.

5. Relative radial abundance ratios

It is well-known that massive early-type galaxies have abundance patterns that do not match that of the solar neighbourhood (see Paper II, and references therein). Although the influence of non-scaled solar abundance ratio patterns complicates the estimation of mean ages from integrated light, it does provide an important clue as to the formation and chemical enrichment histories of galaxies. In this section, we explore the presence of relative abundance ratio gradients in our sample of LDEGs. To do so, we compare the metallicity gradients obtained with different indices (combined with H β) and make the assumption that the differences in the derived values are due to the different sensitivities of the Lick indices to changes in the chemical composition. While avoiding a detailed quantitative analysis (due to the

difficulty in performing this kind of analysis with the current stellar population models, see Paper II for details), the qualitative trends presented below do offer invaluable information concerning the formation of these galaxies and the timescales for star formation therein.

Figure 7 shows three $\Delta\text{index}-\Delta\text{index}$ diagrams in which gradients of CN₂, Mgb, and C4668 are compared to the gradients of Fe4383. The lines corresponding to $\Delta\text{age} = 0$ and $\Delta[\text{M}/\text{H}] = 0$ are overplotted. Due to the low sensitivity to age of all these indices, the diagrams appear highly degenerate – i.e., the iso-age and iso-metallicity lines are almost parallel. If the galaxies did not have a gradient in the relative abundances, we would expect to find all the points distributed along these lines. However, they appear to be systematically shifted toward the left of the diagram, although the magnitude of these shifts is very different in the three plots. In the first panel ($\Delta\text{Mgb}-\Delta\text{Fe4383}$), the metallicity gradients measured with Mgb are slightly steeper than the metallicity gradients inferred from Fe4383, although the differences are admittedly small. In the second panel ($\Delta\text{CN}_2-\Delta\text{Fe4383}$), the differences are more evident. The metallicity gradients obtained with CN₂ are clearly steeper (in absolute value) than the ones inferred from Fe4383. The last panel ($\Delta\text{C4668}-\Delta\text{Fe4383}$) is an intermediate case. The metallicity gradient obtained with C4668 is slightly steeper than the one estimated from Fe4383. Although the trend is not as evident as in the second panel, the points are visibly shifted toward the left of the constant age and metallicity lines.

To analyse these differences in more detail, we calculated the metallicity gradients in several index-index diagrams using the indices CN₂, C4668, Fe4383, Mgb, and Ca4227, combined with H β . In Fig. 8, we compare these gradients with the values obtained from ten different indicators, as described in Sect. 3. Clearly, while the values obtained with Ca4227 and Fe4383 are compatible with the gradients obtained in Sect. 3, the gradients calculated with CN₂, C4668, and, perhaps, Mgb are steeper. We quantified these differences by measuring the mean gradient using the various diagrams, the results of which are summarised in Table 3. The final column of the table shows the probability that the mean gradients calculated with the various indicators are the same as the gradients calculated Sect. 3. The gradients calculated using CN₂ and C4668 are almost twice as steep as the gradients calculated with the average of ten indicators. In the case of Mgb, despite the mean gradient being almost twice as steep as the mean metallicity gradient, the result is less significant. In that case, the initial hypothesis can be rejected with a significance level lower than 0.025.

We could argue that the differences in the metallicities derived with different indicators are due to variations in the

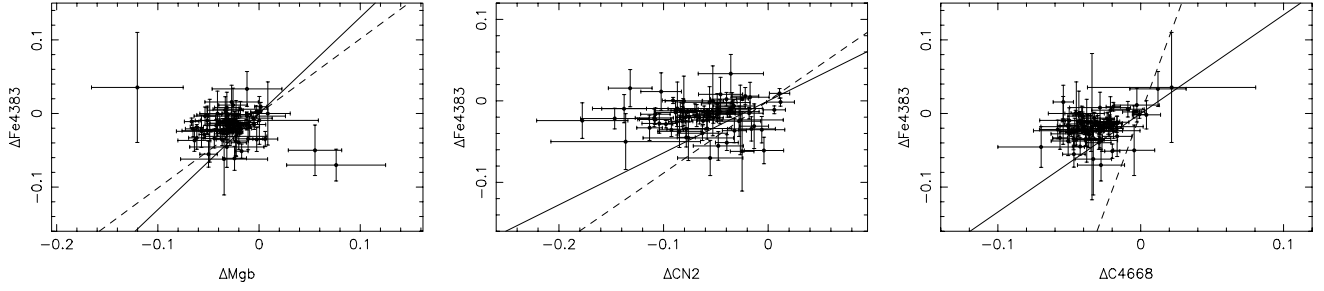


Fig. 7. Δ index– Δ index diagrams in which we compare the Fe4383 gradients with the gradients of Mgb, CN₂, and C4668. Dashed lines indicate the expected gradients if the only parameter varying with radius is the age (assuming an invariant solar metallicity), while solid lines show the expected trends if the only parameter changing with radius is the metallicity (assuming a constant age of 10 Gyr).

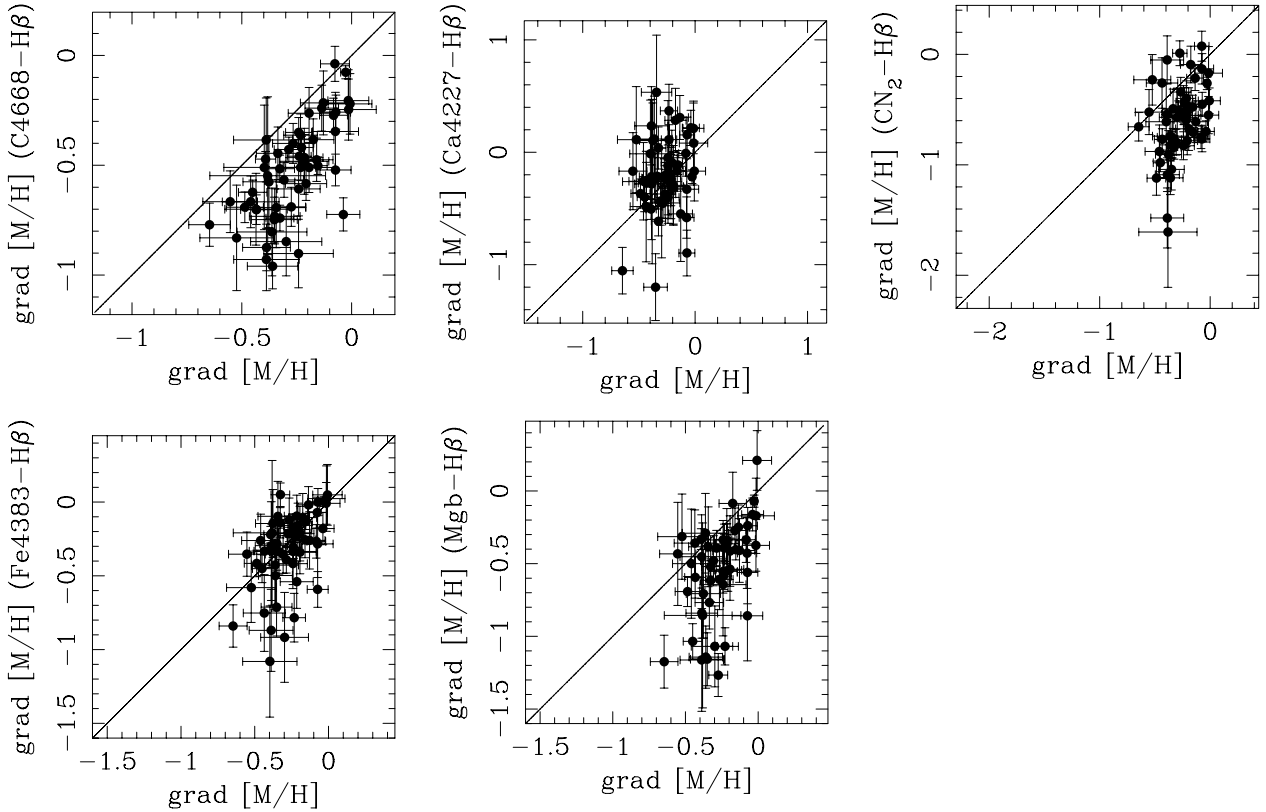


Fig. 8. Comparison of the metallicity gradient measured with different indicators combined with H β , and the metallicity gradient calculated combining ten different indicators (see text for details).

chemical composition as a function of galactocentric distance, as the sensitivity of different Lick indices to variations on the abundance of different chemical elements is not the same (Tripicco & Bell 1995; Korn et al. 2004). But the Lick indices show a dependence on gravity that, while not large (Gorgas et al. 1993; Worthey et al. 1994), is also not null. As the behaviour of each line index under variations in the underlying IMF is not identical, a change in the ratio of dwarf-to-giant stars with galactocentric radius could result in the metallicity gradient inferred from different indicators also being different.

Cenarro et al. (2003) calibrated the CaT* (calcium triplet) index in the near-infrared and found a relationship between [Fe/H], velocity dispersion, and the slope of the IMF. One of the projections of this relationship is

$$\mu = 2.41 + 2.78[\text{M}/\text{H}] - 3.79[\text{M}/\text{H}]^2, \quad (12)$$

where μ represents the slope of the IMF. Using this equation, we determined the slope of the IMF from the average metallicities

in the centre, and at a distance of one effective radius, finding the following values:

- $\mu = 2.56$ in the central regions,
- $\mu = 1.67$ at a distance of one effective radius from the galaxy centre.

To investigate the variation in the line-strength indices that such a variation in the IMF, plus an average variation in metallicity such as that obtained in Sect. 4 would produce, we parameterised the indices (using the V06 models) as a function of metallicity and μ , obtaining:

$$\text{CN}_2 = 0.037 - 0.006\mu + 0.135[\text{M}/\text{H}] + 0.049[\text{M}/\text{H}]^2$$

$$\text{Ca4227} = 1.374 + 0.160\mu + 0.955[\text{M}/\text{H}] + 0.157[\text{M}/\text{H}]^2$$

$$\text{Fe4383} = 5.596 + 0.047\mu + 4.239[\text{M}/\text{H}] + 0.878[\text{M}/\text{H}]^2$$

$$\text{C4668} = 5.593 - 0.294\mu + 6.425[\text{M}/\text{H}] + 1.805[\text{M}/\text{H}]^2$$

$$\text{Mgb} = 3.770 + 0.130\mu + 2.257[\text{M}/\text{H}] + 2.257[\text{M}/\text{H}]^2.$$

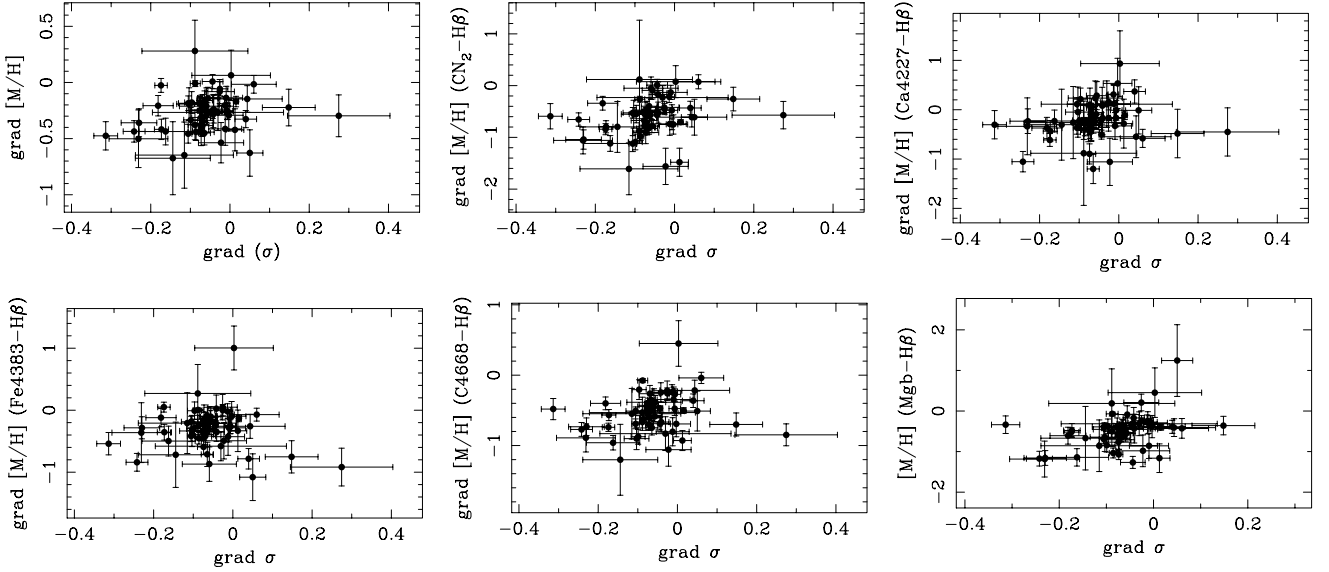


Fig. 9. Relation between the metallicity gradients obtained in different index-index diagrams (as indicated in the brackets) and the velocity dispersion gradient for the sample of LDEGs. In the top left panel, the metallicity gradient has been obtained using a combination of ten indices, as described in Sect. 3.

A variation in the slope of the IMF, together with a variation in metallicity equal to the mean metallicity gradient calculated in Sect. 4, would produce the following differences in the selected indices: $\Delta\text{CN}_2 = 0.0278$ mag, $\Delta\text{Ca4227} = 0.0390$ mag, $\Delta\text{Fe4383} = 0.0264$ mag, $\Delta\text{C4668} = 0.0182$ mag, and $\Delta\text{Mgb} = 0.0270$ mag. The mean observed variations for the LDEGs are: $\Delta\text{CN}_{2\text{obs}} = -0.0662 \pm 0.0096$ mag, $\Delta\text{Ca4227}_{\text{obs}} = -0.0157 \pm 0.0097$ mag, $\Delta\text{Fe4383}_{\text{obs}} = -0.0174 \pm 0.0064$ mag, $\Delta\text{C4668}_{\text{obs}} = -0.0314 \pm 0.0044$ mag, and $\Delta\text{Mgb}_{\text{obs}} = -0.0301 \pm 0.0062$ mag. As can be seen, a variation of the IMF of the form predicted by Cenarro et al. (2003) cannot be responsible for the different metallicity gradients obtained with the various indicators. In fact, this variation of the IMF would produce positive gradients in the selected indices. In this parameterisation, we have not included the effect of age, but the age gradients are not very strong in our sample (see Sect. 4), and the differences in the sensitivities of the analysed indices to this parameter are not enough to produce the observed differences.

More likely, the differences in the metallicity gradients obtained with the different indices are due to changes in the relative abundance gradients of distinct elements. However, it is difficult to quantify the strength of those gradients with the present knowledge of line formation and the inherent limitations of stellar population synthesis models

6. Correlation of the gradients with other parameters

There are several physical processes that can produce a metallicity gradient in early-type galaxies. The relationship between these gradients and other global properties of the galaxies afford an opportunity to discriminate among the competing processes. Previous attempts have searched for correlations using colours and empirical line-strength indices; in what follows, we study the correlation between the gradients of the derived simple stellar population (SSP) parameters and the global properties of the host galaxies. In this section, we only use the subsample of elliptical galaxies, excluding the lenticulars (S0) from the analysis. The reason for doing this is that the correlations between

the gradients and other parameters are predicted by a specific mechanism of galaxy formation, and, although S0 and E galaxies seem to have the same relations between the central properties and other parameters, very different mechanisms have been proposed for their formation. As the sample of S0 is small, we could not perform a comparative study using only S0 galaxies.

6.1. Correlation of the metallicity gradient with the velocity dispersion gradient

As noted in Sect. 1, Franx & Illingworth (1990) found a correlation between colour gradient and the gradient of *escape velocity*, which they interpreted as a correlation between the local metallicity and the local potential well depth in a sample of early-type galaxies. They suggested that such a correlation was consistent with a galactic wind origin, and inconsistent with a dissipative inward flow origin. Others, including Davies et al. (1993), Carollo & Danziger (1994), and Mehlert et al. (2003) find similar relations between the gradients of some line-strength indices and the gradient of the potential well³. We now examine the likelihood of the existence of this correlation within our sample of LDEGs, using the inferred metallicity gradients and empirical velocity dispersion gradients – Fig. 9 illustrates the observed trends.

To study the degree of correlation, we have performed two different tests: a non-parametric Spearman rank order test and a t -test. The Spearman test does not take into account the errors in the individual points, while the t -test has the limitation of considering just a linear relation, and it assumes Gaussian probability distributions. A good estimate of the degree of correlation between both magnitudes can be obtained by studying the results of both tests. In the t -test, we check the hypothesis “ $b = 0$ ”,

³ Davies et al. (2003) calculated the local escape velocity using the surface brightness and the kinematics of the galaxies (Jørgensen et al. 1992). Carollo & Danziger (1994) obtained this parameter with asymmetric dynamical models that depended on the total energy and the angular momentum along the symmetry axis. Mehlert et al. (2003) used the gradient of velocity dispersion as a measure of the local potential well depth.

Table 4. Linear fits and probability of no correlation between the metallicity gradient and the gradient of velocity dispersion. N : number of galaxies in the fit; $b + \sigma(b)$: slope and error of the linear fit (the errors have been calculated by Monte Carlo simulations, as described in the text); t : t -statistic to verify the hypothesis “ $b = 0$ ” (a t value higher than 1.96 allows the hypothesis to be rejected, with a significance level lower than 0.05); Pnc: probability of no correlation in a non-parametric Spearman test.

	N	$b + \sigma(b)$	t	Pnc
grad age	54	1.727 ± 3.099	0.56	0.885
grad [M/H]	54	0.175 ± 0.269	0.65	0.238
grad [M/H] (CN ₂ –H β)	54	1.134 ± 0.555	2.04	0.002
grad [M/H] (Ca4227–H β)	54	0.449 ± 0.686	0.65	0.063
grad [M/H] (Fe4383–H β)	54	-0.392 ± 0.442	0.89	0.900
grad [M/H] (C4668–H β)	54	0.451 ± 0.356	1.27	0.062
grad [M/H] (Mgb–H β)	54	0.876 ± 0.463	2.11	0.001

where b is the slope of the linear fit to the data. The errors in the slope were calculated through Monte Carlo simulations, where each point was perturbed in both axes, assuming a Gaussian distribution with standard deviation equal to the errors. For a significance level of $\alpha = 0.05$, a t value higher than 1.96 indicates that a correlation exists. The results of both tests are shown in Table 4. In the second row of the table (and left top panel in Fig. 9), we show the correlation when the metallicity is measured with the ten indicators described in Sect. 3. We do not find any correlation between the metallicity gradients and the gradient of velocity dispersion. The other panels in the figure show the metallicity gradients obtained in different Δ index– Δ index diagrams in which we combined H β with various metallicity indicators (as indicated between the brackets). Surprisingly, we find a marginally significant correlation between the metallicity gradients and grad σ when the metallicity gradient is measured using Mgb and CN₂ indices, while we do not find any correlation when the metallicity gradient is obtained using the other indices. If the correlation between these parameters is indicative of the importance of galactic winds during the evolution of early-type galaxies, the fact that the correlation only exists when the metallicity gradient is calculated with some specific indices may indicate that this process affects some chemical species more than others. This could happen if, for example, the relative abundance patterns were different when the galactic winds occurred.

The dispersion in the relations is, in any case, very large. This large scatter may be a consequence of using the velocity dispersion as an indicator of the local potential and/or indicative that other processes are driving the variation of the local metal content with radius. Davies et al. (1993), in fact, suggest that the local velocity dispersion is a poor indicator of the local escape velocity, due to the (complicating) presence of rotation and anisotropies. On the other hand, the existence of kinematically decoupled cores in a large percentage of galaxies, the presence of shells, dust lanes, and the observation of interacting galaxies, seem to indicate that mergers and interactions are common processes in the lives of galaxies. If these interactions have some associated gas dissipation and/or star formation, it may produce dispersion in the correlation between local metallicity and local escape velocity. In fact, other authors (Davies et al. 1993; Carollo & Danziger 1994) have found correlations between the Mg₂ and the velocity dispersion gradients using the local escape velocity instead of the velocity dispersion, also finding a large scatter in the relations.

We conclude that the local potential of early-type galaxies may play a role in defining the metallicity gradient. However, the large scatter in the derived correlation suggests that other processes may play a role in modulating the final metal content. These processes can be the consequence of differences in the merger histories of galaxies, as proposed by Kobayashi (2004).

The fact that the inferred metallicity gradients differ depending upon the indicator adopted also suggests that the gradients of the various chemical species have probably been formed (and modified) through different physical mechanisms.

6.2. Correlation of the metallicity gradient with the central velocity dispersion

Dissipative collapse models of galaxy formation predict strong correlations between the metallicity gradients and certain global parameters, such as the luminosity, mass, and central velocity dispersion (Larson 1974a; Carlberg 1984; Arimoto & Yoshii 1987; Kawata 1999; Chiosi & Carraro 2002; Kawata & Gibson 2003), in the sense that more massive galaxies should possess steeper metallicity gradients. Such a prediction is driven primarily by the adopted mass-dependent feedback efficiency within the models. Conversely, galaxy formation through hierarchical clustering of small sub-units does not necessarily lead to a clear prediction of any putative correlations between metallicity gradients and global galactic properties – merger history can readily play a part in eroding any extant correlation (e.g., Kobayashi 2004).

With the aim of exploring the possible correlation between metallicity gradient and galactic mass, we compare the metallicity gradients (obtained as described in Sect. 3) with the central velocity dispersion for the sample of LDEGs in Fig. 10. The other panels in the figure show the relation between the metallicity gradient and the central velocity dispersion when the metallicity gradient is measured using CN₂, C4668, Fe4383, Mgb, and Ca4227 combined with H β .

As in Sect. 6.1, we studied the degree of correlation through a t -test and a non-parametric Spearman test. The results of these tests are shown in Table 5. We did not find any correlation between the metallicity gradients and the central velocity dispersion, regardless of the line-strength indices used to derive the former.

In regards to putative correlations between line-strength indices and the mass or the velocity dispersion, Peletier (1989), Peletier et al. (1990), and G90, each found positive correlations between the Mg₂ gradient and the central velocity dispersion, while González (1993) and Davies & Sadler (1987) found the opposite trend. Conversely, Davidge (1991, 1992) and Davies et al. (1993) did not find any correlation between the gradients of the indices Mg₂, $\langle \text{Fe} \rangle$, or H β and the central velocity dispersion. In this work, we have doubled the sample size compared to any of the extant studies, and instead of analysing the colours or raw line-strength gradients, we employed the inferred metallicity gradients. For the sample of LDEGs, we did not find any correlation between these parameters and the central velocity dispersion.

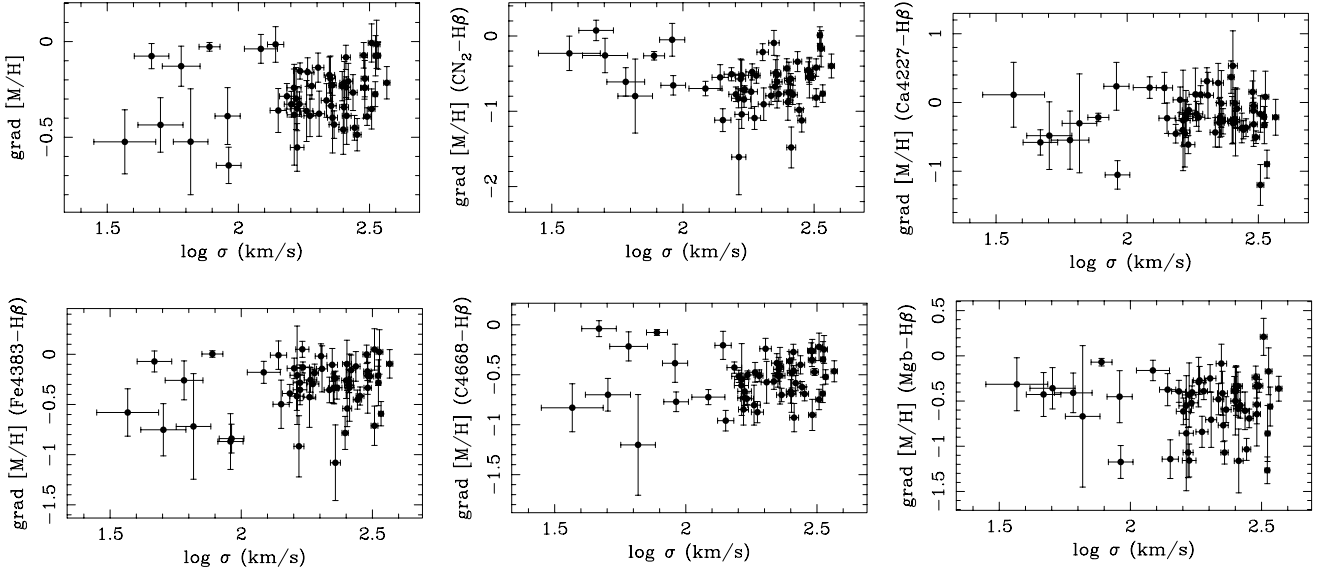


Fig. 10. Metallicity gradients obtained in different index-index diagrams (as indicated in brackets) versus the central velocity dispersion.

Table 5. Correlation between the gradients of age and metallicity and the central velocity dispersion. The brackets show the different indicators used to calculate the metallicity gradients. The first and the second rows refer to the values calculated using the ten indicators described in Sect. 3. t : t -parameter calculated as the quotient of the slope and its error, computed through Monte Carlo simulations; Pnc: probability of no correlation according to a non-parametric Spearman test.

	N	t	Pnc
grad age	54	-1.736	0.168
grad [M/H]	54	0.810	0.106
grad [M/H] (CN ₂ -H β)	54	1.075	0.789
grad [M/H] (Ca4227-H β)	54	0.251	0.986
grad [M/H] (Fe4383-H β)	54	1.303	0.244
grad [M/H] (C4668-H β)	54	0.026	0.455
grad [M/H] (Mgb-H β)	54	0.578	0.934

6.3. Correlation of the gradients with the age of the central regions

In Sect. 6.1, we showed that, for the sample of LDEGs, the metallicity gradients tend to correlate with the velocity dispersion gradient when they are measured with *some* indicators (in particular CN₂ and Mgb), but that this correlation disappears when the metallicity gradient is measured with Fe4383, Ca4227, and C4668.

In Sect. 4 we showed that the mean age gradient in our sample of LDEGs is not null, which might be indicative of the occurrence of star formation events in the centre of the galaxies. Furthermore, we showed in Paper II that in these events, the relative enrichment of some chemical species (the ones mainly released by low- and intermediate-mass stars, like Fe) might be more important than others (the ones mainly produced in type II supernovae, like Mg). With the aim of exploring whether the occurrence of star formation processes in the centre of the galaxies may be responsible for the abundance gradients in some chemical species, we now study the correlation between the metallicity gradients and the central ages obtained in Paper II. Figure 11 shows these correlations for different measurements of the metallicity gradient. When the correlation is statistically significant, a linear fit taking into account the errors in the x - and y -directions is also plotted. In these cases, the probability of

no correlation (Pnc) obtained in a non-parametric Spearman test and the t parameter to verify the hypothesis $b = 0$ (where b is the slope of the linear fit) are indicated in the panels. As can be seen in the different panels, while we do not find any significant correlation when the metallicity gradients are measured with CN₂, Mgb, or Ca4227, we *do* find a correlation between the metallicity gradients and the central age of the galaxies, when the former is measured using Fe4383 and C4668. We also find a significant correlation between the metallicity gradient obtained with the ten indicators described in Sect. 3 and the central age of the galaxies. We interpret these correlations in Sect. 6.4.

6.4. Interpretation of the correlations for the LDEGs

In Sects. 6.1–6.3, we studied the putative correlations between metallicity gradient and other global properties of LDEGs. Broadly speaking, we found two distinct characteristics of the gradients depending upon the specific indicator used to derive them:

- *Metallicity gradients measured with CN₂ and Mgb.* These correlate with the velocity dispersion gradient, but they do not correlate with the central velocity dispersion or with the central age of the galaxies. This behaviour may indicate that the gradients of some elements (in particular Mg and N) are the result of processes such as galactic winds, which can develop after an intense burst of star formation in the earliest phases of galaxy formation. The possible subsequent star formation in the galaxies has not substantially modified the variation of these elements with radius. This is in agreement with the results of Papers I and II, where we argued that the relative enrichment of Fe in the star formation processes which occurred in the centre of the galaxies had to be more important than that of Mg.
- *Metallicity gradients measured with Fe4383 and C4668.* These gradients do not correlate with the velocity dispersion gradient, but they do correlate with the central age of the galaxy. The correlation with the central age may indicate that episodes of star formation in the centre of the galaxies considerably affects the metallicity gradient for these chemical species, increasing the central metallicity.

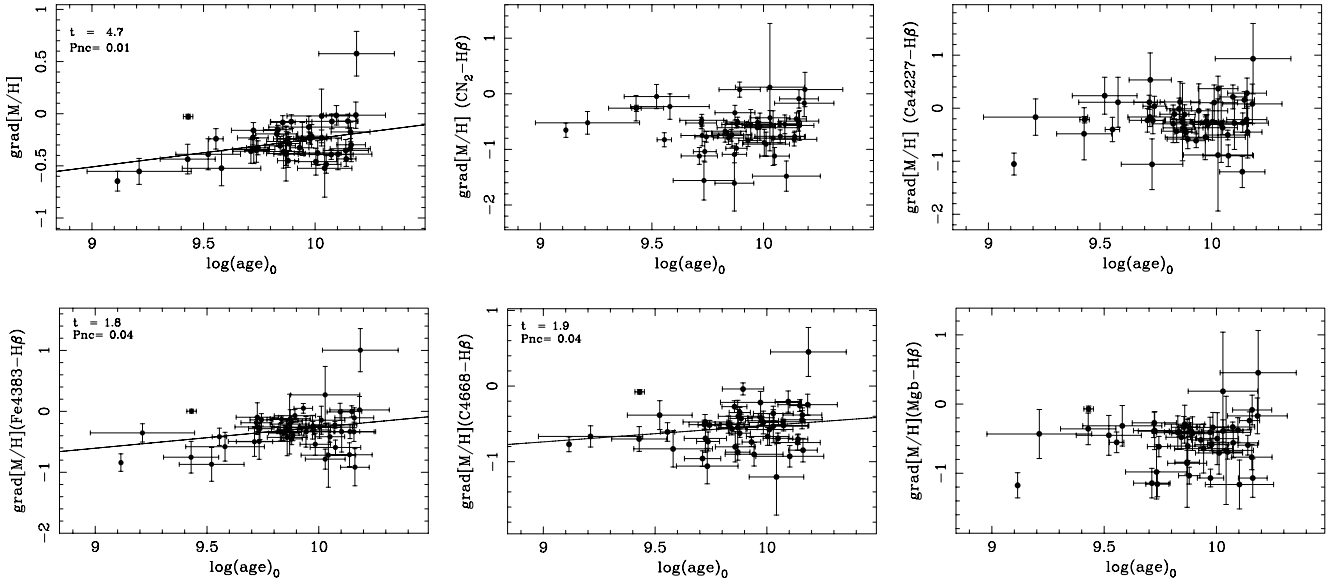


Fig. 11. Relation of the metallicity gradient to the central age of the galaxies. When the correlation is statistically significant, a linear fit weighted by the errors in both axes is also shown. In these cases, the t parameter and the probability of no correlation (Pnc), as derived from a non-parametric Spearman rank test, are also indicated in the top-left corner of the panels. For a significance level of 0.05, a value of t larger than 1.96 indicates the presence of correlation between both variables.

This view agrees with the results of Papers I and II. Note that in galaxies that have suffered star formation episodes in their centres, the $[\text{Mg}/\text{Fe}]$ gradient flattens as a consequence of the Fe enrichment in the central parts, which is supported by the relation between $[\text{Mg}/\text{Fe}]$ and age reported in Paper I. This is also in agreement with the result presented in Paper II, in which we found the existence of an age-metallicity relation when the metallicity was measured with Fe4383, but not when this parameter was measured with Mgb.

Conversely, in Sánchez-Blázquez et al. (2003), we reported differences in the N abundance between galaxies in different environments. If the star formation processes in the centres of the galaxies do not substantially affect the gradients in this element, then the differences must be visible not only in the centres, but also in the outer parts.

We also note the behaviour of the metallicity gradient when inferred from Ca4227. Specifically, the gradient does not correlate with any of the obvious physical parameters – i.e., neither with the central age nor with the velocity dispersion gradient.

7. Global stellar population parameters

Many of the results described in Papers I and II could be explained by assuming the presence of a small percentage of young stars in the centre of most of the galaxies, at least in the subsample of LDEGs. We have also argued that this could be the cause of the existence of non-null age gradients in our sample of galaxies (see Sect. 4). If this point of view is correct, we would expect that the relations defined between the global parameters of the galaxies (i.e., for the whole bodies of the galaxies) are different than the one derived for the central regions. To investigate this possibility, we now compare for the subsample of LDEGs, the relation of these global values and the velocity dispersion with the relations derived for the central values in Paper II. The *global*

values can be obtained from the gradients, assuming a linear behaviour of the indices with radius and evaluating the integral

$$I_{\text{global}} = \frac{\int_0^\infty I(r) 2\pi I_e \exp^{-7.67[(r/r_e)^{1/4}-1]} dr}{\int_0^\infty 2\pi I_e \exp^{-7.67[(r/r_e)^{1/4}-1]} dr}, \quad (13)$$

where $I(r) = a + b \log(r/r_e)$ represents the index at a distance r from the galaxy, as derived from the gradient, and r_e is the effective radius. To solve this integral, we have assumed that the spatial profile of the galaxies can be approximated with a de Vaucouleurs law.

Figure 12 shows the relation between the global age and global metallicities (as derived from different indicators) and the central velocity dispersion. We plot a linear fit to the data weighted with the errors in both parameters, and to compare with the relations for the central regions, we have also plotted the linear fits obtained for the central values derived in Paper II. Table 6 summarises the parameters of the fits. We carried out a t -test to verify the existence of significant differences between the slopes of the trends defined by the central and the global SSP-parameters. A value of t higher than 1.96 indicates that there exist differences with a significance level lower than 0.05.

The only case in which the slopes defined by the central and the global values are significantly different is in the relation between the age and the central velocity dispersion. While the central age shows a significant correlation with the central velocity dispersion (see Paper II), the global age, as derived in this section, does not correlate with this parameter. This result favours the idea that, in a large percentage of galaxies, the young ages that we found in Paper II are due to a minor percentage of stars that formed in the centre of the galaxies at a later epoch than the bulk of the stars, as suggested by Trager et al. (2000b). It also supports the suggestion that this minor percentage of young stars in the centre of the galaxies is responsible for the age gradients reported in Sect. 4.

Table 6. Parameters of the linear fits, weighted with errors, of the age and metallicities (measured in different index-index diagrams indicated between brackets) and the central velocity dispersion. The table shows the results for the central values (a_c and b_c) and for the global values (a_g and b_g). The coefficients a and b represent the zero point and the slope of the linear fit, respectively. The last column shows the t parameter obtained in a t -test to check the hypothesis $b_c = b_g$. A value of t higher than 2.326 allows us to reject the hypothesis with a significance level lower than 0.01.

	Central		Global		
	a_c	b_c	a_g	b_g	t
[M/H] (CN ₂ -H β)	0.335 ± 0.081	0.00037 ± 0.00034	-0.012 ± 0.091	0.00080 ± 0.00038	0.86
[M/H] (Fe4383-H β)	0.148 ± 0.064	-0.00050 ± 0.00030	-0.275 ± 0.226	0.00041 ± 0.00087	0.98
[M/H] (Mgb-H β)	0.113 ± 0.075	0.00112 ± 0.00031	-0.427 ± 0.286	0.00212 ± 0.00107	0.88
log age	9.534 ± 0.075	0.00177 ± 0.00033	9.950 ± 0.115	0.00007 ± 0.00049	2.88

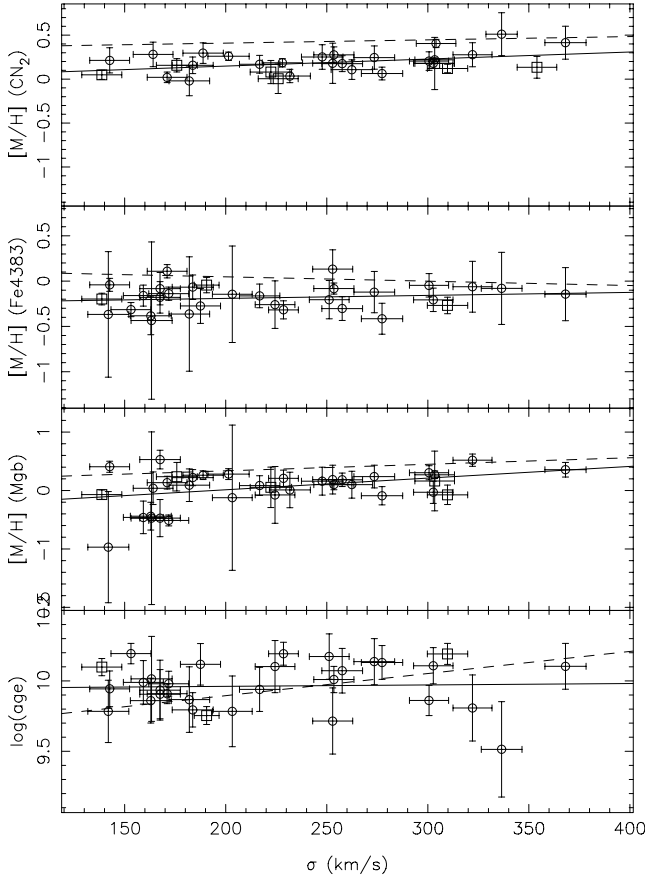


Fig. 12. Relation between the global age and metallicity and the central velocity dispersion for galaxies in low-density environments. The solid line represents a linear fit weighted with the errors for the global data. The dashed line indicates the fit obtained for the central values reported in Paper II. Open circles represent E galaxies, while the S0 are represented by squares.

On the other hand, the slopes of the relations between the metallicity and the central velocity dispersion do not show a statistically significant variation between the central and the global values, although there is a tendency for the relations to be steeper for the global values. There are also differences in the zero point as a consequence of the existence of gradients, in disagreement with the earlier claims of González & Gorgas (1996). These authors found that the relation $Mg_2 - \sigma$ is flatter at one effective radii than in the center, concluding that the mass-metallicity relation was much flatter at one effective radii than in the central parts of the galaxies. In light of our present series of papers, the results of González & Gorgas could be explained if the

differences between the central and global relation of the age with σ was causing these differences.

The lack of variation in the slope of the relation between the central and the global metallicities measured with CN₂ and Mgb was expected, since we find a flat relation between the strength of the gradients and the central velocity dispersion. In the case of the metallicity measured with Fe4383, we might have expected to see a steepening of the slope in the global relation compared with the central one. If the relative importance of the star formation processes has been higher in the smaller galaxies (as suggested by the age- σ relation), the metallicity inferred from Fe4383 in these galaxies should be also higher. The variation in the slope obtained when comparing the central and the global relations goes in this sense, but the differences are not statistically significant. We must note that the errors in the global measurements are higher than for the central values, which might explain the lack of statistical significance.

8. Differences in the gradients as a function of environment

If the environment in which galaxies reside has any influence over the timescales of the star formation, the number of interactions, or the dissipation of gas, we might expect to see an environmental dependence upon the inferred age and metallicity gradients. Fisher et al. (1995) analysed a sample of bright cluster ellipticals, concluding that their gradients and those of field ellipticals, were not significantly different. When studying the photometry in the B - and R -bands as a function of radius for galaxies in Abell 2199, Tamura & Otha (2003) found correlations between the colour gradients and some global properties of the galaxies, such as the luminosity and effective radius, which had not been found in studies of field galaxies. These authors, however, only found these correlations amongst the most luminous galaxies ($R < 15$ mag and with an effective radius $> 3''$). We now examine the mean gradients of the SSP-parameters for the HDEGs and compare these values with the ones obtained for the LDEGs.

8.1. Mean stellar population gradients in HDEGs

The second column of Table 7 lists the mean values of the SSP-parameter gradients obtained for the HDEGs in different index-index diagrams (indicated between brackets). As in Sect. 4, we quantified the probability that these values are different from zero by chance. The results of a t -test indicate that, while the metallicity gradients obtained in the CN₂-H β and C4668-H β diagrams are not compatible with being null, the metallicity gradients obtained in the Fe4383-H β and Ca4227-H β diagrams are compatible with zero, within the

Table 7. Mean stellar population gradients and their errors for HDEGs. σ : standard deviation about the mean; N : number of galaxies averaged; N_{eff} : effective number of points; t : t -statistic to verify the hypothesis “mean = 0”; σ_{exp} : standard deviation expected from the errors; α : significance level to reject the hypothesis “ $\sigma = \sigma_{\text{exp}}$ ” in a χ^2 test. Column 9 shows the t -statistic to confirm whether the gradients obtained with individual indicators are the same as the metallicity gradients obtained with a combination of ten different indicators. As a reference, the 10th column shows the mean gradients obtained for the LDEGs from Sect. 4 (see Table 3). The final column of the table shows the t -statistic, to verify if the mean gradients are the same for both samples of galaxies, LDEGs and HDEGs. A high value of t indicates significant differences.

	Mean	σ	N	N_{eff}	t	σ_{exp}	α	t	LDEGs	t'
grad log age	0.027 ± 0.067	0.258	15	9.79	0.34	0.138	0.0003		0.082 ± 0.015	0.8
grad [M/H]	-0.328 ± 0.064	0.247	15	11.85	5.59	0.157	0.0017		-0.206 ± 0.019	1.8
grad [M/H] (CN ₂ –H β)	-0.643 ± 0.111	0.432	15	10.86	5.60	0.236	0.0003	2.10	-0.582 ± 0.032	0.5
grad [M/H] (C4668–H β)	-0.599 ± 0.092	0.358	15	9.18	5.71	0.185	4.2E–06	1.96	-0.459 ± 0.028	1.4
grad [M/H] (Fe4383–H β)	-0.168 ± 0.118	0.456	15	8.95	1.47	0.275	0.0014	0.95	-0.197 ± 0.025	0.2
grad [M/H] (Mgb–H β)	-0.537 ± 0.158	0.611	15	10.23	2.85	0.337	4.2E–05	1.02	-0.407 ± 0.039	0.8
grad [M/H] (Ca4227–H β)	-0.168 ± 0.214	0.831	15	11.16	0.70	0.434	1.7E–06	0.61	-0.238 ± 0.034	0.3

errors. Furthermore, the mean age gradient for this subsample of galaxies is also compatible with zero. We now analyse these results separately:

- *Age gradient.* If we assume that the most likely scenario to explain the age gradient in early-type galaxies is the occurrence of star formation processes in the centres of these systems, the lack of a mean age gradient in the HDEGs indicates that these galaxies have undergone few episodes of star formation in recent times, when compared with field galaxies. If the star formation processes are triggered by the interactions between galaxies, the differences could be explained due to the lower probability of an interaction in the centre of the Coma cluster. This is in agreement with the conclusions of Papers I and II, where we showed that the central stellar populations of the Coma cluster galaxies possessed, on average, older ages than the LDEGs.
- *Metallicity gradients.* The mean metallicity gradient obtained for this subsample of galaxies is $\Delta[\text{M}/\text{H}]/\log r = -0.328 \pm 0.064$, slightly steeper than the gradient obtained for the LDEGs. From her simulations, Kobayashi (2004) predicts a metallicity gradient for galaxies that have not suffered major mergers of $\Delta \log Z / \Delta \log r \sim -0.3$. These predictions are in agreement with the mean values obtained for the galaxies in the Coma cluster. On the other hand, as for the LDEGs, the metallicity gradients are steeper when obtained with some indicators (CN₂, C4668, and Mgb), although the statistical significance of the differences is much lower than in the case of the LDEGs (see final column of Table 7). This may also be due to the larger errors in the determination of the gradients for the galaxies in the Coma cluster.

We next checked to see if the scatter amongst the mean values was compatible with the dispersion expected by the errors. We carried out a χ^2 test of the hypothesis $\sigma = \sigma_{\text{exp}}$ (where σ is the observed scatter and σ_{exp} the scatter expected from the errors), to see whether it could be rejected with a low significance level (α). Column 8 of Table 7 shows the α values resulting from this test. We find a real scatter in both the age and the metallicity gradients that cannot be explained by the errors, in contrast with the findings of Mehlert et al. (2003). The difference may be due to the fact that the sample used by Mehlert et al. spans a more limited range in velocity dispersion ($2.2 < \log \sigma < 2.5$).

8.2. Correlation of the metallicity gradients in HDEGs with the central velocity dispersion

According to Kobayashi (2004), the absence of correlation between the metallicity gradient and the central velocity dispersion

may be the consequence of differences in the merger history of the galaxies. If the star formation processes in recent epochs have been less frequent in the Coma cluster galaxies, one might expect that any in situ correlation would have been less substantially impacted. To explore whether this is the case, in Fig. 13 we present the metallicity gradients measured in different $\Delta \text{index} - \Delta \text{index}$ diagrams against the central velocity dispersion for the elliptical galaxies of the Coma cluster. The table at the bottom of the figure shows the results of a t -test and a non-parametric Spearman rank test to check the degree of correlation between both variables. In this case, we find a correlation between the metallicity gradient and the central velocity dispersion, but only when the metallicity gradient is measured with the Fe4383 index. While the correlation is not statistically significant when derived from other indices, there does seem to be a marginal trend in the sense that more massive galaxies also show a steeper gradient. To confirm this putative mass trend and further constrain galaxy formation models, higher signal-to-noise spectra must be obtained.

9. Conclusions

We have carried out a study of the gradients in 23 different spectral features for a sample of 82 early-type galaxies situated in different environments. Our results can be summarised thus:

- Using the new synthesis stellar population models of V06 we derived age and metallicity gradients for all the galaxies in the sample. We used a new method that employs ten different indicators to reduce the scatter due to random errors.
- The mean age and metallicity gradients for the LDEGs are $\Delta[\text{M}/\text{H}]/\log r = -0.205 \pm 0.075$ and $\Delta \log(\text{age})/\log r = 0.082 \pm 0.032$, respectively. The mean age gradient is steeper and the mean metallicity gradient flatter than the predictions of dissipative collapse models. On the other hand, the dispersion amongst the mean values is larger than the dispersion expected by errors alone.
- We studied the metallicity gradients derived from different indicators, obtaining steeper gradients when using CN₂ and C4668 than with Fe4383 and Ca4227. Although it is beyond the scope of this paper to derive chemical abundance ratio gradients, we speculate that these aforementioned differences reflect the existence of radial variations in the relative abundances of some elements with respect to iron.
- We studied the relation between the age and metallicity gradients and the gradient of velocity dispersion, finding a correlation when the metallicity gradient is calculated with CN₂ and Mgb. We do not, however, find a correlation when

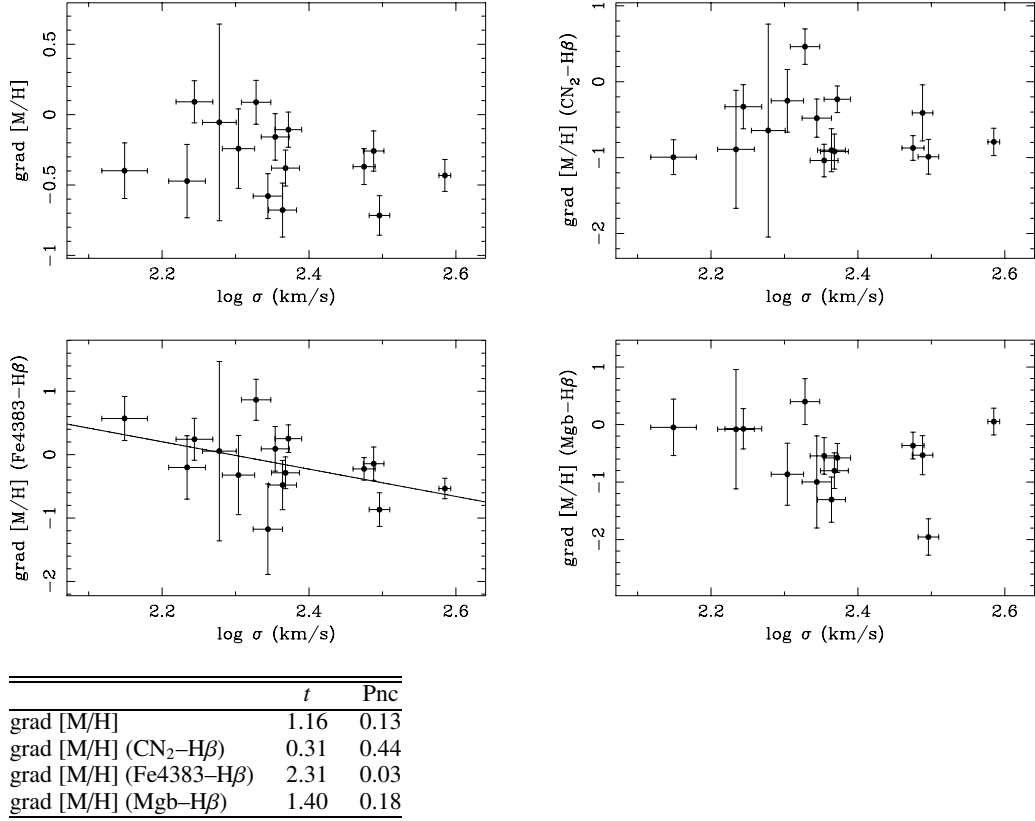


Fig. 13. Metallicity gradients versus central velocity dispersion for HDEGs. The different panels show the metallicity gradients obtained in different index-index diagrams (indicated between the brackets). The first panel (*top left*) compares the metallicity gradients obtained as described in Sect. 3. In the case in which the correlation is statistically significant, an error weighted linear fit is also shown. The table at the bottom indicates the results of a t -test and a non-parametric Spearman rank test (see text for details).

the metallicity gradient is derived from the Fe4383 and Ca4227 indices. The fact that the gradients of CN₂ and Mgb correlate with the gradient of the velocity dispersion may indicate that the gradients in some elements (e.g. N, and Mg) were shaped early in the formation of galaxies, when the galactic winds presumably dominate. On the other hand, the lack of correlation when using Fe4383 and Ca4227 to measure the metallicity can indicate that other process, such as secondary bursts of star formation, have had a stronger influence in the final shape of these gradients.

- We have not found any correlation between the metallicity gradients and the central velocity dispersion for the sample of galaxies in low-density environments. A strong correlation between the gradients and the mass of the galaxy is expected within dissipative collapse formation scenarios.
- We found a significant correlation between the metallicity gradients and the central age for the LDEGs, when the metallicity gradients are measured with Fe4383 and C4668, in the sense that galaxies with a younger central age also show a steeper metallicity gradient.
- The results quoted above suggest that the gradients of different chemical species may have formed by different mechanisms.
- The mean age and metallicity gradients for the galaxies in the Coma cluster are $\Delta \log(\text{age})/\log r = 0.027 \pm 0.138$ and $\Delta [\text{M}/\text{H}]/\log r = -0.328 \pm 0.157$, respectively. The mean value of the age gradient is compatible with zero, to within the errors. Both values are also compatible with the predictions of Kobayashi (2004), for those galaxies that have not undergone major mergers. However, the dispersion amongst

the mean values is higher than the scatter expected by the errors, indicative of real differences between galaxies.

- For galaxies in the Coma cluster, we studied the correlation between the metallicity gradients and the central velocity dispersion, finding a statistically significant correlation between both parameters when the metallicity is measured with Fe4383. For the other indices, the correlation is not statistically significant, but we observe a trend in the sense that more massive galaxies tend to have a steeper metallicity gradient. This trend is predicted by models of dissipative collapse and was not found for the LDEGs. We should stress, though, that the quality of the data for the HDEGs is lower than that for the LDEGs; higher quality data for the Coma cluster galaxies are urgently needed. In any case, in this paper we found systematic differences between the stellar populations of galaxies in different environments, which both confirm *and* extend our conclusions from Papers I and II.

Acknowledgements. We would like to thank the anonymous referee for very helpful comments. The WHT is operated on the island of La Palma by the Royal Greenwich Observatory at the Observatorio del Roque de los Muchachos of the Instituto de Astrofísica de Canarias. The Calar Alto Observatory is operated jointly by the Max-Planck Institute für Astronomie, Heidelberg, and the Spanish Instituto de Astrofísica de Andalucía (CSIC). This work was partially supported by the Spanish research project AYA 2003-01840 and by the Australian Research Council. We are grateful to the CATs for their generous allocations of telescope time.

References

- Arimoto, N., & Yoshii, Y. 1987, *A&A*, 173, 23
 Barnes, J. E., & Hernquist, L. E. 1991, *ApJ*, 370, L65

- Baugh, C. M., Cole, S., & Frenk, C. S. 1996, *MNRAS*, 283, 1361
- Bender, R., & Surma, P. 1992, *A&A*, 258, 250
- Binney, J. 1978, *MNRAS*, 183, 501
- Borison, T. A., & Thompson, I. B. 1991, *AJ*, 101, 111
- Bekki, K., & Shioya, Y. 1999, *ApJ*, 513, 108
- Burstein, D. 1979, *ApJ*, 232, 74
- Cardiel, N., Gorgas, J., & Aragón-Salamanca, A. 1998a, *MNRAS*, 298, 977
- Cardiel, N., Gorgas, J., Cenarro, J., & González, J. J. 1998b, *A&AS*, 127, 597
- Carlberg, R. G. 1984, *ApJ*, 286, 403
- Carollo, C. M., & Danziger, I. J. 1994, *MNRAS*, 270, 523
- Carollo, C. M., Danziger, I. J., & Buson, L. 1993, *MNRAS*, 265, 553
- Cenarro, A. J., Gorgas, J., Vazdekis, A., Cardiel, N., & Peletier, R. F. 2003, *MNRAS*, 339, L12
- Cohen, J. G. 1979, *ApJ*, 228, 405
- Chiosi, C., & Carraro, G. 2002, *MNRAS*, 335, 335
- Cole, S., Aragón-Salamanca, A., Frenk, C. S., Navarro, J. F., & Zepf, S. E. 1994, *MNRAS*, 271, 781
- Couture, J., & Hardy, E. 1988, *AJ*, 96, 867
- Davidge, T. J. 1991, *AJ*, 102, 896
- Davidge, T. J. 1992, *AJ*, 103, 1512
- Davies, R. L., & Sadler, E. M. 1987, *Structure and Dynamics of Elliptical Galaxies*, ed. T. de Zeeuw (Dordrecht: Reidel), IAU Symp., 127, 441
- Davies, R. L., Sadler, E. M., & Peletier, R. F. 1993, *MNRAS*, 262, 650
- Efstathiou, G., & Gorgas, J. 1985, *MNRAS*, 215, P37
- Eggen, O. J., Lynden-Bell, D., & Sandage, A. R. 1962, *ApJ*, 136, 748
- Faber, S. M., Friel, E. D., Burstein, D., & Gaskell, C. M. 1985, *ApJS*, 57, 711
- Fisher, D., Franx, M., & Illingworth, G. 1995, *ApJ*, 448, 119
- Fisher, D., Franx, M., & Illingworth, G. 1996, *ApJ*, 459, 110
- Franx, M., & Illingworth, G. 1990, *ApJ*, 359, L41
- Franx, M., Illingworth, G., & Heckman, T., 1989, *AJ*, 98, 538
- Gibson, B. K. 1997, *MNRAS*, 290, 471
- González, J. J. 1993, Ph.D. Thesis, University of California
- González, J. J., & Gorgas, J. 1996, in *Fresh Views of Elliptical Galaxies*, ed. A. Buzzoni, A. Renzini, & A. Serrano (San Francisco: ASP) ASP Conf. Ser., 86., 225
- Gorgas, J., Efstathiou, G., & Aragón-Salamanca, A. 1990, *MNRAS*, 245, 217 (G90)
- Gorgas, J., Faber, S. M., Burstein, D., et al. 1993, *ApJS*, 86, 153
- Gorgas, J., Pedraz, S., Guzmán, R., Cardiel, N., & González, J. J. 1997, *ApJ*, 481, L19
- Joly, M., & Andriolat, Y. 1973, *A&A*, 26, 95
- Jørgensen, I., Franx, M., & Kjærgaard, P. 1992, *A&AS*, 95, 489
- Kauffmann, G. 1996, *MNRAS*, 281, 487
- Kauffmann, G., & Charlot, S. 1998, *MNRAS*, 294, 705
- Kawata, D. 1999, *PASJ*, 51, 931
- Kawata, D., & Gibson, B. 2003, *MNRAS*, 346, 135
- Kobayashi, C. 2004, *MNRAS*, 347, 740
- Kobayashi, C., & Arimoto, N. 1999, *ApJ*, 527, 573
- Kormendy, J., & Djorgovski, S. 1989, *ARA&A*, 27, 235
- Larson, R. B. 1974a, *MNRAS*, 166, 585
- Larson, R. B. 1974b, *MNRAS*, 169, 229
- Larson, R. B. 1975, *MNRAS*, 173, 671
- Mathews, W. G., & Baker, J. C. 1971, *ApJ*, 170, 241
- Martinelli, A., Matteucci, F., & Colafrancesco, S. 1998, *MNRAS*, 298, 42
- McClure, R. D. 1969, *AJ*, 74, 50
- Mehlert, D., Thomas, D., Saglia, R. P., Bender, R., & Wegner, G. 2003, *A&A*, 407, 423
- Mihos, J. C., & Hernquist, L. 1994, *ApJ*, 427, 112
- Mould, J. R. 1978, *ApJ*, 220, 434
- Munn, J. A. 1992, *ApJ*, 399, 444
- Oke, J. B., & Schwarzschild, M. 1975, *ApJ*, 198, 630
- Peletier, R. F. 1989, Ph.D. Thesis, University of Groningen
- Peletier, R. F., Davies, R. L., Illingworth, G. D., Davis, L. E., & Cawson, M. 1990, *AJ*, 100, 1091
- Sánchez-Blázquez, P. 2004, Ph.D. Thesis, Universidad Complutense de Madrid
- Sánchez-Blázquez, P., Gorgas, J., Cardiel, N., Cenarro, A. J., & González, J. J. 2003, *ApJ*, 590, L91
- Sánchez-Blázquez, P., Gorgas, J., Cardiel, N., & González, J. J. 2006a, *A&A*, 457, 787 (Paper I)
- Sánchez-Blázquez, P., Gorgas, J., Cardiel, N., & González, J. J. 2006b, *A&A*, 457, 809 (Paper II)
- Sánchez-Blázquez, P., Peletier, R. F., Jiménez, J., et al. 2006c, *MNRAS* [arXiv:astro-ph/0607009]
- Spinrad, H., Smith, H. E., & Taylor, D. J. 1972, *ApJ*, 175, 649
- Spinrad, H., Gunn, J. E., Taylor, B. J., McClure, R. D., & Young, J. W. 1971, *ApJ*, 164, 11
- Schweizer, F., Seitzer, P., Faber, S. M., et al. 1990, *ApJ*, 364, L33
- Tamura, N., & Ohta, K. 2003, *AJ*, 126, 596
- Thomas, D., Maraston, C., & Bender, R. 2003, *MNRAS*, 339, 897
- Thomsen, B., & Baum, W. A. 1989, *ApJ*, 347, 214
- Trager, S. C., Worthey, G., Faber, S. M., Burstein, D., & González, J. J. 1998, *ApJS*, 116, 1
- Trager, S. C., Faber, S. M., Worthey, G., & González, J. J. 2000a, *AJ*, 119, 1645
- Trager, S. C., Faber, S. M., Worthey, G., & González, J. J. 2000b, *AJ*, 120, 165
- van Albada, T. S. 1982, *MNRAS*, 201, 939
- Vazdekis, A. 1999, *ApJ*, 513, 224
- Welch, G. A., & Forrester, W. T. 1972, *AJ*, 77, 333
- White, S. D. M. 1980, *MNRAS*, 191, 1
- Worthey, G. 1994, *ApJS*, 95, 107
- Worthey, G., Faber, S. M., González, J. J., & Burstein, D. 1994, *ApJS*, 94, 687

Online Material

Table 1. Velocity dispersion and line-strength gradients for the sample of 82 galaxies. A portion of the table is shown for guidance regarding its form and content. For each galaxy and index, the first line shows the measured gradient, while the second row lists its corresponding formal error. The full table is available in the electronic edition of this paper.

Nombre	σ	D4000	H δ_A	H δ_F	CN ₂	Ca4227	G4300	Hy _A	Hy _F	Fe4383
NGC 221	-0.0877	-0.0520	-0.0014	0.0008	-0.0247	-0.0110	0.0104	0.0018	0.0079	0.0025
	0.0126	0.0058	0.0023	0.0026	0.0057	0.0035	0.0025	0.0020	0.0032	0.0017
NGC 315	-0.0439	-0.2038	0.0111	-0.0016	0.0059	-0.0081	-0.0112	0.0424	0.0454	-0.0110
	0.0261	0.0177	0.0048	0.0064	0.0106	0.0076	0.0056	0.0057	0.0058	0.0048
NGC 507	0.0029	0.0276	0.0182	0.0179	-0.0357	0.0123	0.0526	-0.0447	-0.0676	0.0334
	0.0992	0.0554	0.0124	0.0293	0.0312	0.0425	0.0296	0.0142	0.0250	0.0236
NGC 584	-0.0769	-0.1955	0.0331	0.0312	-0.0655	-0.0139	-0.0001	0.0313	0.0394	-0.0204
	0.0326	0.0582	0.0123	0.0108	0.0191	0.0210	0.0144	0.0124	0.0205	0.0079
NGC 636	-0.0121	-0.2441	0.0243	0.0285	-0.0848	-0.0011	-0.0226	0.0419	0.0405	-0.0374
	0.0416	0.0483	0.0159	0.0221	0.0207	0.0222	0.0168	0.0164	0.0158	0.0198
NGC 821	-0.0226	-0.2749	0.0480	0.0225	-0.1467	-0.0506	-0.0113	0.0251	0.0310	-0.0217
	0.0570	0.0602	0.0257	0.0277	0.0326	0.0220	0.0106	0.0119	0.0155	0.0127
NGC 1453	-0.0419	-0.0769	0.0332	0.0342	-0.0583	-0.0387	0.0060	0.0191	0.0162	-0.0339
	0.0224	0.0284	0.0150	0.0242	0.0234	0.0209	0.0163	0.0105	0.0148	0.0130
NGC 1600	-0.0739	-0.1825	0.0146	-0.0017	-0.0484	-0.0234	-0.0054	0.0182	0.0171	-0.0150
	0.0155	0.0098	0.0079	0.0080	0.0107	0.0116	0.0068	0.0050	0.0068	0.0067
NGC 1700	-0.0031	-0.0787	0.0170	-0.0115	-0.0813	0.0303	-0.0075	0.0141	0.0078	-0.0098
	0.0362	0.0294	0.0176	0.0183	0.0144	0.0298	0.0147	0.0146	0.0152	0.0125
NGC 2300	-0.1032	0.0088	0.0154	0.0100	-0.0490	0.0060	0.0086	0.0090	-0.0097	-0.0165
	0.0312	0.0697	0.0205	0.0222	0.0228	0.0276	0.0186	0.0175	0.0222	0.0091
NGC 2329	0.0502	0.0548	0.0254	0.0266	-0.0554	0.0077	0.0018	0.0310	0.0193	-0.0701
	0.0330	0.0491	0.0313	0.0323	0.0312	0.0229	0.0262	0.0219	0.0142	0.0216
NGC 2693	-0.0259	-0.1256	0.0118	0.0110	-0.0683	-0.0373	-0.0063	0.0156	0.0166	-0.0181
	0.0370	0.0300	0.0118	0.0127	0.0098	0.0152	0.0159	0.0080	0.0109	0.0135
NGC 2694	-0.0885	-0.9690	0.0647	0.0246	-0.0138	-0.0843	0.0306	0.0153	0.0842	-0.0036
	0.1337	0.1819	0.1381	0.1250	0.1186	0.0576	0.0660	0.0667	0.1095	0.0056
NGC 2778	-0.2297	-0.2964	0.0425	0.0342	-0.1089	-0.0156	-0.0357	0.0415	0.0486	-0.0209
	0.0450	0.0141	0.0120	0.0115	0.0182	0.0132	0.0120	0.0210	0.0243	0.0109
NGC 2832	-0.0646	-0.1193	0.0226	-0.0094	-0.0783	-0.0689	-0.0244	0.0357	0.0162	-0.0448
	0.0152	0.0154	0.0087	0.0148	0.0086	0.0166	0.0084	0.0090	0.0097	0.0118
NGC 3115	-0.1056	-0.3075	0.0232	0.0146	-0.1086	-0.0149	-0.0098	0.0223	0.0194	-0.0228
	0.0094	0.0114	0.0051	0.0063	0.0160	0.0068	0.0118	0.0127	0.0092	0.0054
NGC 3377	-0.1624	-0.2541	0.0292	0.0025	-0.1134	-0.0116	-0.0320	0.0368	0.0280	-0.0331
	0.0672	0.0324	0.0102	0.0120	0.0122	0.0085	0.0063	0.0108	0.0136	0.0155
NGC 3379	-0.0737	-0.1927	0.0184	0.0155	-0.0556	-0.0189	-0.0194	0.0245	0.0216	-0.0189
	0.0087	0.0072	0.0042	0.0046	0.0057	0.0046	0.0056	0.0044	0.0044	0.0038
NGC 3605	-0.0594	-0.2601	0.0111	0.0386	-0.0040	0.0163	0.0285	0.0384	0.0284	-0.0609
	0.0683	0.0458	0.0235	0.0224	0.0188	0.0171	0.0239	0.0223	0.0175	0.0163
NGC 3608	-0.0728	-0.1859	0.0460	0.0438	-0.1081	-0.0085	0.0129	0.0128	0.0003	-0.0226
	0.0329	0.0349	0.0180	0.0141	0.0149	0.0107	0.0132	0.0092	0.0123	0.0061
NGC 3641	-0.1151	-0.5179	0.0831	0.0703	-0.1777	-0.0281	-0.0341	0.0213	0.0707	-0.0242
	0.1236	0.0703	0.0307	0.0356	0.0436	0.0326	0.0344	0.0522	0.0542	0.0218
NGC 3665	-0.0557	-0.0052	0.0029	0.0120	-0.0182	0.0087	-0.0057	0.0110	-0.0014	-0.0151
	0.0260	0.0289	0.0113	0.0155	0.0134	0.0136	0.0109	0.0069	0.0118	0.0071
NGC 3818	-0.0992	-0.2511	0.0304	0.0266	-0.1078	-0.0080	-0.0222	0.0275	0.0349	-0.0164
	0.0176	0.0169	0.0079	0.0101	0.0141	0.0097	0.0099	0.0119	0.0133	0.0078
NGC 4261	-0.0663	-0.0881	0.0090	0.0085	-0.0578	-0.0096	-0.0263	0.0279	0.0197	-0.0138
	0.0089	0.0100	0.0054	0.0064	0.0055	0.0106	0.0064	0.0066	0.0070	0.0044
NGC 4278	-0.0856	-0.2121	0.0441	0.0484	-0.0978	-0.0208	-0.0138	0.0457	0.0604	-0.0286
	0.0082	0.0072	0.0044	0.0051	0.0066	0.0060	0.0072	0.0053	0.0068	0.0047
NGC 4365	-0.0606	-0.2294	0.0092	0.0122	-0.0623	-0.0193	-0.0069	0.0272	0.0304	-0.0247
	0.0123	0.0086	0.0054	0.0067	0.0061	0.0065	0.0058	0.0052	0.0067	0.0043
NGC 4374	-0.0255	-0.1773	0.0138	0.0136	-0.0612	-0.0056	-0.0132	0.0185	0.0343	-0.0125
	0.0201	0.0210	0.0097	0.0097	0.0113	0.0098	0.0082	0.0065	0.0084	0.0062
NGC 4415	0.0602	-0.0585	-0.0050	0.0052	0.0118	-0.0325	0.0177	0.0124	0.0326	-0.0015
	0.0565	0.0205	0.0092	0.0106	0.0133	0.0095	0.0101	0.0096	0.0126	0.0050
NGC 4431	0.0436	-0.0467	0.0015	-0.0349	-0.0398	-0.0094	-0.0083	-0.0052	0.0023	0.0021
	0.0881	0.0406	0.0176	0.0212	0.0153	0.0240	0.0115	0.0074	0.0134	0.0083
NGC 4464	-0.0967	-0.2536	0.0101	0.0017	-0.0700	-0.0004	0.0036	0.0179	0.0273	-0.0119
	0.0177	0.0155	0.0115	0.0125	0.0166	0.0125	0.0110	0.0282	0.0280	0.0082
NGC 4467	-0.1443	-0.2577	0.0208	-0.0265	-0.0763	-0.0122	0.0095	0.0448	0.0375	-0.0455
	0.0946	0.0724	0.0263	0.0318	0.0433	0.0340	0.0346	0.0788	0.0896	0.0277
NGC 4472	-0.0436	-0.1140	0.0212	0.0118	-0.0563	-0.0320	0.0011	0.0084	0.0026	-0.0156
	0.0063	0.0069	0.0029	0.0034	0.0042	0.0051	0.0039	0.0034	0.0037	0.0033

Table 1. continued.

Nombre	σ	D4000	H δ_A	H δ_F	CN ₂	Ca4227	G4300	H γ_A	H γ_F	Fe4383
NGC 4478	-0.0727	-0.1332	0.0076	-0.0058	-0.0389	-0.0139	-0.0161	0.0074	0.0000	-0.0157
	0.0240	0.0086	0.0059	0.0065	0.0073	0.0062	0.0100	0.0119	0.0111	0.0043
NGC 4486B	-0.2310	-0.7128	0.0064	0.0056	-0.0806	0.0103	-0.0028	0.0045	-0.0057	-0.0001
	0.0742	0.1373	0.0282	0.0459	0.0179	0.0297	0.0431	0.0440	0.0535	0.0305
NGC 4489	0.1483	-0.4048	0.0159	0.0018	-0.0061	-0.0082	-0.0216	0.0234	0.0109	-0.0354
	0.0666	0.0773	0.0219	0.0149	0.0220	0.0302	0.0135	0.0076	0.0160	0.0162
NGC 4552	-0.0572	-0.1592	0.0284	0.0098	-0.0817	-0.0063	0.0030	0.0059	-0.0004	-0.0117
	0.0183	0.0258	0.0110	0.0148	0.0112	0.0174	0.0095	0.0102	0.0127	0.0088
NGC 4564	-0.1740	-0.1850	0.0019	-0.0082	-0.0909	-0.0427	-0.0078	0.0096	0.0145	0.0005
	0.0157	0.0185	0.0062	0.0061	0.0103	0.0066	0.0068	0.0075	0.0084	0.0038
NGC 4594	0.0126	-0.2270	0.0490	0.0307	-0.1377	-0.0005	0.0081	0.0286	0.0554	-0.0096
	0.0224	0.0257	0.0097	0.0158	0.0214	0.0249	0.0138	0.0226	0.0212	0.0173
NGC 4621	-0.0720	-0.1734	0.0134	0.0036	-0.0755	-0.0126	0.0060	0.0239	0.0125	-0.0198
	0.0080	0.0120	0.0070	0.0070	0.0081	0.0096	0.0061	0.0050	0.0059	0.0061
NGC 4636	-0.0742	-0.1762	0.0200	0.0287	-0.0363	0.0024	-0.0125	0.0256	0.0246	-0.0109
	0.0262	0.0322	0.0139	0.0142	0.0176	0.0168	0.0109	0.0066	0.0135	0.0089
NGC 4649	-0.0641	-0.0489	0.0044	0.0229	-0.0477	-0.0205	-0.0105	0.0228	0.0260	-0.0123
	0.0198	0.0257	0.0133	0.0159	0.0165	0.0163	0.0134	0.0090	0.0110	0.0095
NGC 4673	-0.3136	-0.1806	0.0593	0.0560	-0.0487	-0.0530	-0.0324	0.0424	0.0583	-0.0036
	0.0519	0.0138	0.0143	0.0169	0.0152	0.0187	0.0122	0.0088	0.0075	0.0124
NGC 4692	-0.0808	-0.1060	0.0231	0.0380	-0.0885	-0.0235	-0.0171	0.0218	0.0166	-0.0142
	0.0601	0.0161	0.0183	0.0287	0.0198	0.0163	0.0166	0.0111	0.0147	0.0130
NGC 4697	0.0151	-0.2025	0.0303	0.0181	-0.0771	-0.0112	-0.0137	0.0244	0.0293	-0.0126
	0.0065	0.0221	0.0033	0.0042	0.0041	0.0049	0.0035	0.0028	0.0029	0.0032
NGC 4742	-0.2420	-0.1593	-0.1027	-0.1252	0.0109	0.0183	0.0351	-0.0901	-0.1320	0.0092
	0.0276	0.0122	0.0129	0.0138	0.0097	0.0083	0.0103	0.0261	0.0303	0.0059
NGC 4839	-0.0423	-0.1857	0.0492	0.0356	-0.0134	0.0385	-0.0116	0.0433	0.0002	-0.0311
	0.1146	0.0319	0.0335	0.0355	0.0138	0.0359	0.0264	0.0208	0.0183	0.0274
NGC 4842A	-0.2731	-0.0902	-0.0263	-0.0614	-0.1362	0.0771	-0.0711	0.0325	-0.0027	-0.0500
	0.1125	0.0600	0.0441	0.0239	0.0715	0.0284	0.0474	0.0423	0.0267	0.0343
NGC 4864	-0.0010	-0.0811	-0.0179	0.0077	-0.0249	-0.0171	-0.0135	0.0477	0.0329	-0.0620
	0.1205	0.0244	0.0238	0.0304	0.0113	0.0258	0.0284	0.0265	0.0166	0.0487
NGC 4865	-0.2596	-0.1158	-0.0129	-0.0221	-0.0461	0.0030	0.0139	-0.0172	-0.0081	-0.0132
	0.0400	0.0238	0.0319	0.0507	0.0374	0.0190	0.0158	0.0157	0.0257	0.0150
NGC 4874	0.0810	-0.1949	0.0412	0.0643	-0.0345	-0.0317	-0.0074	-0.0228	-0.0631	-0.0021
	0.0772	0.0258	0.0155	0.0204	0.0171	0.0188	0.0131	0.0129	0.0198	0.0121
NGC 4875	-0.2320	0.0183	-0.0267	-0.0331	-0.0529	-0.0152	0.0297	0.0081	-0.0117	0.0000
	0.0774	0.0547	0.0068	0.0437	0.0102	0.0703	0.0138	0.0239	0.0402	0.0429
NGC 4889	-0.0708	-0.1506	-0.0005	0.0119	-0.0785	0.0128	0.0151	0.0131	0.0127	-0.0347
	0.0309	0.0163	0.0098	0.0112	0.0183	0.0188	0.0114	0.0069	0.0125	0.0103
NGC 4908	-0.1810	-0.1450	0.0389	0.0763	-0.0266	0.0384	-0.0588	0.0644	0.0381	-0.0234
	0.1363	0.0397	0.0225	0.0595	0.0410	0.0488	0.0488	0.0302	0.0423	0.0427
NGC 5638	-0.0690	-0.1999	0.0264	0.0256	-0.0820	0.0007	-0.0220	0.0265	0.0313	-0.0114
	0.0124	0.0092	0.0072	0.0084	0.0078	0.0099	0.0082	0.0081	0.0105	0.0046
NGC 5796	-0.1814	-0.1352	0.0026	-0.0154	-0.0340	-0.0221	0.0009	0.0046	0.0048	-0.0074
	0.0381	0.0201	0.0095	0.0117	0.0121	0.0115	0.0125	0.0112	0.0151	0.0083
NGC 5812	-0.1731	-0.2445	0.0294	0.0124	-0.0822	-0.0272	-0.0233	0.0342	0.0261	-0.0250
	0.0176	0.0118	0.0076	0.0078	0.0102	0.0116	0.0101	0.0119	0.0129	0.0067
NGC 5813	-0.0064	-0.2948	0.0364	0.0268	-0.0791	-0.0023	-0.0193	0.0333	0.0363	-0.0203
	0.0146	0.0153	0.0070	0.0074	0.0090	0.0109	0.0069	0.0069	0.0089	0.0056
NGC 5831	-0.0694	-0.2808	0.0503	0.0362	-0.0925	-0.0326	-0.0379	0.0546	0.0576	-0.0355
	0.0261	0.0150	0.0112	0.0131	0.0115	0.0129	0.0106	0.0077	0.0109	0.0083
NGC 5845	-0.3136	-0.3665	0.0338	0.0286	-0.0628	-0.0208	-0.0211	0.0380	0.0239	-0.0397
	0.0300	0.0199	0.0135	0.0096	0.0237	0.0145	0.0152	0.0196	0.0218	0.0090
NGC 5846	0.0398	-0.1676	0.0012	-0.0230	-0.0395	0.0292	-0.0188	0.0216	0.0144	-0.0512
	0.0273	0.0089	0.0073	0.0082	0.0109	0.0128	0.0065	0.0054	0.0083	0.0097
NGC 5846A	0.2745	-0.1974	0.0027	0.0086	-0.0477	-0.0162	-0.0379	0.0397	0.0215	-0.0553
	0.1293	0.0336	0.0141	0.0121	0.0239	0.0281	0.0134	0.0110	0.0185	0.0176
NGC 6127	-0.0884	-0.2386	0.0328	0.0337	-0.0840	-0.0085	-0.0098	0.0316	0.0385	-0.0122
	0.0171	0.0173	0.0245	0.0234	0.0248	0.0206	0.0139	0.0090	0.0100	0.0107
NGC 6166	-0.0096	-0.0327	0.0270	0.0022	-0.0323	-0.0411	-0.0172	0.0325	0.0209	-0.0366
	0.0415	0.0209	0.0121	0.0148	0.0115	0.0148	0.0154	0.0100	0.0131	0.0148
NGC 6411	-0.0067	-0.2148	0.0135	-0.0137	-0.0524	-0.0136	-0.0132	0.0259	0.0351	-0.0207
	0.0146	0.0116	0.0088	0.0123	0.0095	0.0094	0.0058	0.0054	0.0079	0.0068
NGC 6482	-0.0696	-0.0383	0.0253	-0.0017	-0.0586	-0.0305	0.0066	0.0259	0.0335	-0.0236
	0.0270	0.0310	0.0147	0.0152	0.0146	0.0183	0.0125	0.0092	0.0124	0.0101

Table 1. continued.

Nombre	σ	D4000	H δ_A	H δ_F	CN $_2$	Ca4227	G4300	H γ_A	H γ_F	Fe4383
NGC 6702	-0.0410	-0.1912	0.0227	0.0342	-0.0327	0.0126	0.0003	0.0246	0.0241	-0.0063
	0.0196	0.0130	0.0164	0.0165	0.0200	0.0204	0.0137	0.0090	0.0117	0.0079
NGC 6703	-0.1053	-0.1916	0.0189	0.0176	-0.0577	0.0038	-0.0267	0.0253	0.0171	-0.0160
	0.0246	0.0166	0.0043	0.0060	0.0100	0.0072	0.0062	0.0054	0.0043	0.0051
NGC 7052	-0.0136	-0.1008	0.0054	0.0106	-0.0368	0.0040	0.0163	0.0138	0.0393	-0.0140
	0.0134	0.0212	0.0071	0.0100	0.0093	0.0099	0.0080	0.0064	0.0070	0.0061
NGC 7332	-0.0232	-0.3047	0.0199	0.0106	-0.0871	-0.0020	-0.0208	0.0248	0.0237	-0.0256
	0.0178	0.0170	0.0039	0.0046	0.0080	0.0076	0.0059	0.0045	0.0050	0.0058
IC 767	1.4466	-0.4829	-0.0025	-0.0427	0.0133	0.0050	0.0442	-0.0333	-0.0516	-0.0179
	2.3182	0.0591	0.0376	0.0736	0.0443	0.0360	0.0056	0.0415	0.0392	0.0994
IC 794	-0.0303	-0.1679	0.0388	0.0525	-0.0160	0.0157	-0.0148	0.0244	0.0222	-0.0344
	0.1655	0.0347	0.0132	0.0185	0.0229	0.0293	0.0250	0.0197	0.0307	0.0149
IC 832	-0.1324	0.0138	-0.0158	-0.0387	-0.0560	-0.0128	0.0029	-0.0081	-0.0179	-0.0018
	0.0556	0.0410	0.0241	0.0258	0.0263	0.0431	0.0177	0.0153	0.0228	0.0192
IC 3957	-0.0347	-0.5857	0.0493	-0.0335	-0.0868	-0.1265	-0.0755	0.0577	0.0492	-0.0094
	0.0895	0.1203	0.0312	0.0572	0.0812	0.0323	0.1151	0.0680	0.0887	0.0325
IC 3959	-0.2640	-0.2479	0.0296	0.0259	-0.1023	-0.0299	-0.0377	0.0549	0.0535	0.0114
	0.1392	0.0275	0.0139	0.0268	0.0194	0.0310	0.0253	0.0227	0.0273	0.0230
IC 3963	-0.0381	-0.1294	0.0271	0.0248	-0.0278	-0.0665	0.0030	0.0238	0.0063	-0.0250
	0.1324	0.0293	0.0134	0.0189	0.0207	0.0284	0.0234	0.0109	0.0176	0.0186
IC 3973	-0.3219	-0.3314	-0.0182	-0.0551	-0.0219	0.0161	0.0247	-0.0368	-0.0530	0.0058
	0.0698	0.0733	0.0274	0.0440	0.0129	0.0344	0.0264	0.0220	0.0291	0.0106
IC 4042	-0.2280	-0.5860	0.0509	0.0194	-0.0288	0.0369	-0.0669	0.0307	-0.0079	0.0550
	0.1406	0.1258	0.1236	0.0971	0.2025	0.0791	0.0343	0.0412	0.0746	0.2003
IC 4051	0.0864	-0.2565	0.0545	0.0231	-0.1041	0.0015	-0.0420	0.0385	0.0134	-0.0277
	0.0540	0.0333	0.0127	0.0128	0.0165	0.0262	0.0137	0.0153	0.0173	0.0120
CGCG159-041	-0.2040	-0.2805	0.1211	0.0866	-0.0309	0.0743	0.1851	-0.0545	0.0136	0.0354
	0.2762	0.2039	0.0616	0.0416	0.1286	0.0289	0.1133	0.0343	0.0534	0.0748
CGCG159-043	-0.1134	-0.2382	0.0185	0.0453	-0.0455	-0.0001	0.0001	0.0151	0.0218	0.0080
	0.1105	0.0371	0.0195	0.0265	0.0211	0.0321	0.0205	0.0166	0.0255	0.0209
CGCG159-083	-0.2836	0.3389	-0.0502	-0.0509	-0.0173	0.0039	0.0388	-0.0289	-0.0064	0.0045
	0.1301	0.0403	0.0133	0.0151	0.0182	0.0152	0.0149	0.0148	0.0152	0.0183
CGCG159-089	-0.0218	-0.3534	0.0459	0.0544	-0.1319	0.0219	0.0137	-0.0226	0.0096	0.0156
	0.0885	0.0636	0.0270	0.0266	0.0209	0.0317	0.0284	0.0238	0.0291	0.0228

Table 1. continued.

Galaxia	Ca4455	Fe4531	C4668	H β	Fe5015	Mg ₁	Mg ₂	Mgb	Fe5270	Fe5335
NGC 221	0.0027	-0.0030	-0.0037	-0.0021	0.0052	-0.0007	0.0092	-0.0017	-0.0038	0.0020
	0.0019	0.0016	0.0017	0.0016	0.0019	0.0011	0.0022	0.0018	0.0011	0.0017
NGC 315	0.0113	-0.0275	-0.0396	-0.0039	-0.0045	0.0030	-0.0247	-0.0666	0.0040	-0.0210
	0.0059	0.0051	0.0051	0.0048	0.0040	0.0031	0.0044	0.0072	0.0036	0.0057
NGC 507	-0.0034	0.0150	0.0121	0.0352	0.0279	0.0160	0.0346	-0.0119	0.0013	-0.0026
	0.0206	0.0215	0.0197	0.0109	0.0180	0.0147	0.0225	0.0345	0.0246	0.0241
NGC 584	-0.0120	-0.0113	-0.0290	-0.0036	0.0000	-0.0126	-0.0206	-0.0193	-0.0144	-0.0197
	0.0109	0.0076	0.0065	0.0071	0.0105	0.0061	0.0110	0.0120	0.0071	0.0094
NGC 636	-0.0136	0.0028	-0.0508	0.0064	-0.0227	-0.0216	-0.0482	-0.0230	-0.0012	-0.0106
	0.0176	0.0117	0.0119	0.0095	0.0078	0.0129	0.0162	0.0124	0.0080	0.0119
NGC 821	-0.0227	-0.0302	-0.0581	-0.0124	-0.0222	-0.0472	-0.0765	-0.0417	-0.0084	-0.0129
	0.0073	0.0145	0.0128	0.0167	0.0099	0.0169	0.0197	0.0143	0.0105	0.0148
NGC 1453	-0.0073	-0.0018	-0.0286	0.0328	-0.0143	-0.0080	-0.0148	-0.0442	-0.0218	-0.0061
	0.0165	0.0111	0.0076	0.0098	0.0113	0.0088	0.0114	0.0111	0.0133	0.0159
NGC 1600	-0.0311	0.0005	-0.0206	-0.0251	0.0086	-0.0074	-0.0172	-0.0048	-0.0320	-0.0271
	0.0085	0.0045	0.0039	0.0055	0.0038	0.0085	0.0064	0.0114	0.0088	0.0135
NGC 1700	-0.0101	-0.0073	-0.0426	0.0027	-0.0143	-0.0270	-0.0392	-0.0243	-0.0069	-0.0116
	0.0149	0.0075	0.0102	0.0114	0.0086	0.0078	0.0097	0.0106	0.0087	0.0157
NGC 2300	0.0035	0.0006	-0.0511	-0.0068	0.0005	0.0063	-0.0087	-0.0288	-0.0073	0.0071
	0.0139	0.0141	0.0073	0.0150	0.0083	0.0112	0.0113	0.0131	0.0188	0.0096
NGC 2329	-0.0250	-0.0266	-0.0278	-0.0064	-0.0233			0.0762		
	0.0239	0.0107	0.0165	0.0169	0.0099			0.0489		
NGC 2693	-0.0147	-0.0132	-0.0216	0.0199	-0.0019	-0.0258	-0.0260	-0.0093	-0.0056	-0.0048
	0.0130	0.0074	0.0082	0.0065	0.0063	0.0104	0.0100	0.0098	0.0070	0.0126
NGC 2694	-0.0546	-0.0403	-0.0407	0.0211	0.0128	0.0700	0.0416	-0.0119	-0.0029	0.0259
	0.0911	0.0194	0.0029	0.0318	0.0160	0.0396	0.0400	0.0380	0.0182	0.0170
NGC 2778	-0.0279	-0.0233	-0.0441	0.0006	-0.0212			-0.0653		
	0.0098	0.0099	0.0071	0.0072	0.0072			0.0075		
NGC 2832	-0.0060	-0.0193	-0.0424	-0.0055	-0.0140			0.2740		
	0.0104	0.0068	0.0055	0.0079	0.0092			0.0698		
NGC 3115	-0.0268	-0.0111	-0.0387	-0.0063	-0.0219			-0.0320		
	0.0059	0.0045	0.0041	0.0037	0.0039			0.0046		
NGC 3377	-0.0246	-0.0041	-0.0565	-0.0022	-0.0219	-0.0669	-0.1011	-0.0615	-0.0146	-0.0201
	0.0095	0.0072	0.0052	0.0091	0.0050	0.0062	0.0096	0.0081	0.0069	0.0100
NGC 3379	-0.0169	-0.0102	-0.0258	0.0017	-0.0174	-0.0669	-0.1011	-0.0615	-0.0146	-0.0201
	0.0040	0.0029	0.0028	0.0035	0.0030	0.0052	0.0060	0.0065	0.0053	0.0052
NGC 3605	-0.0095	-0.0028	-0.0226	-0.0010	-0.0392			-0.0242		
	0.0136	0.0104	0.0111	0.0114	0.0103			0.0118		
NGC 3608	-0.0278	-0.0170	-0.0392	0.0113	-0.0263	-0.0527	-0.0788	-0.0514	-0.0151	-0.0135
	0.0160	0.0136	0.0117	0.0147	0.0082	0.0093	0.0062	0.0082	0.0128	0.0079
NGC 3641	-0.0453	-0.0086	-0.0364	0.0086	-0.0386			-0.0569		
	0.0306	0.0259	0.0195	0.0264	0.0144			0.0248		
NGC 3665	-0.0169	-0.0168	-0.0259	0.0070	-0.0086	-0.0242	-0.0212	-0.0122	-0.0009	-0.0086
	0.0126	0.0082	0.0044	0.0094	0.0065	0.0052	0.0076	0.0076	0.0050	0.0065
NGC 3818	-0.0114	-0.0226	-0.0505	-0.0043	-0.0238			-0.0424		
	0.0078	0.0071	0.0060	0.0070	0.0068			0.0068		
NGC 4261	-0.0087	-0.0042	-0.0216	0.0015	-0.0211			-0.0203		
	0.0073	0.0117	0.0036	0.0048	0.0040			0.0059		
NGC 4278	-0.0245	-0.0178	-0.0359	-0.0033	-0.0244			-0.0543		
	0.0045	0.0036	0.0028	0.0048	0.0038			0.0050		
NGC 4365	-0.0238	-0.0166	-0.0286	0.0027	-0.0200			-0.0356		
	0.0052	0.0036	0.0027	0.0036	0.0036			0.0038		
NGC 4374	-0.0147	-0.0077	-0.0203	0.0115	-0.0075	-0.0190	-0.0322	-0.0255	-0.0088	-0.0066
	0.0081	0.0051	0.0048	0.0027	0.0053	0.0042	0.0055	0.0067	0.0052	0.0063
NGC 4415	-0.0137	-0.0031	-0.0009	-0.0033	-0.0143	0.0012	-0.0156	-0.0204	-0.0149	-0.0142
	0.0078	0.0079	0.0045	0.0056	0.0047	0.0115	0.0169	0.0129	0.0080	0.0129
NGC 4431	0.0059	-0.0076	-0.0049	-0.0190	0.0062	-0.0033	0.0037	-0.0028	-0.0299	-0.0046
	0.0125	0.0103	0.0078	0.0110	0.0101	0.0076	0.0126	0.0054	0.0080	0.0094
NGC 4464	-0.0155	-0.0079	-0.0167	0.0104	-0.0116			-0.0319		
	0.0066	0.0091	0.0084	0.0061	0.0062			0.0080		
NGC 4467	0.0296	-0.0208	-0.0697	-0.0053	-0.0226			-0.0318		
	0.0094	0.0373	0.0303	0.0255	0.0250			0.0367		
NGC 4472	-0.0220	-0.0113	-0.0282	-0.0001	-0.0148			-0.0184		
	0.0036	0.0025	0.0019	0.0024	0.0024			0.0034		
NGC 4478	-0.0131	-0.0078	-0.0209	-0.0112	-0.0094			-0.0101		
	0.0045	0.0042	0.0029	0.0048	0.0046			0.0051		

Table 1. continued.

Galaxia	Ca4455	Fe4531	C4668	H β	Fe5015	Mg ₁	Mg ₂	Mgb	Fe5270	Fe5335
NGC 4486B	0.0072	-0.0062	-0.0433	-0.0237	0.0002	0.1090	0.0839	-0.0411	-0.0130	-0.0313
	0.0429	0.0229	0.0098	0.0184	0.0262	0.0257	0.0102	0.0174	0.0043	0.0039
NGC 4489	-0.0292	-0.0076	-0.0348	-0.0168	-0.0208	-0.0031	-0.0160	-0.0023	-0.0218	-0.0298
	0.0098	0.0097	0.0094	0.0099	0.0104	0.0260	0.0206	0.0083	0.0101	0.0136
NGC 4552	-0.0061	-0.0066	-0.0351	0.0004	-0.0084	-0.0362	-0.0533	-0.0309	-0.0103	-0.0047
	0.0074	0.0071	0.0040	0.0064	0.0051	0.0047	0.0054	0.0051	0.0049	0.0059
NGC 4564	-0.0022	-0.0111	-0.0455	0.0028	-0.0109			-0.0320		
	0.0049	0.0040	0.0033	0.0042	0.0029			0.0046		
NGC 4594	-0.0137	-0.0169	-0.0501	-0.0130	-0.0084			-0.0512		
	0.0091	0.0068	0.0056	0.0162	0.0106			0.0118		
NGC 4621	-0.0152	-0.0115	-0.0405	-0.0036	-0.0150			-0.0294		
	0.0061	0.0032	0.0035	0.0055	0.0041			0.0059		
NGC 4636	-0.0335	-0.0186	-0.0216	-0.0120	-0.0134	-0.0201	-0.0287	-0.0302	-0.0108	-0.0062
	0.0111	0.0060	0.0069	0.0069	0.0086	0.0071	0.0066	0.0079	0.0066	0.0083
NGC 4649	-0.0190	0.0037	-0.0300	0.0051	-0.0124	-0.0263	-0.0404	-0.0257	0.0052	0.0089
	0.0090	0.0066	0.0063	0.0042	0.0058	0.0043	0.0057	0.0069	0.0056	0.0078
NGC 4673	-0.0006	-0.0103	-0.0407	0.0199	-0.0096	-0.0239	-0.0599	-0.0534	-0.0239	-0.0262
	0.0127	0.0090	0.0103	0.0095	0.0105	0.0041	0.0064	0.0108	0.0080	0.0105
NGC 4692	-0.0231	-0.0088	-0.0417	-0.0057	-0.0141	-0.0392	-0.0588	-0.0388	0.0055	-0.0205
	0.0061	0.0169	0.0119	0.0124	0.0096	0.0082	0.0091	0.0123	0.0107	0.0081
NGC 4697	-0.0096	-0.0094	-0.0313	0.0030	-0.0137			-0.0257		
	0.0030	0.0022	0.0023	0.0024	0.0020			0.0032		
NGC 4742	-0.0113	-0.0036	-0.0192	-0.0637	-0.0164			0.0017		
	0.0082	0.0055	0.0050	0.0082	0.0054			0.0060		
NGC 4839	-0.0311	-0.0394	-0.0080	-0.0165	-0.0261	-0.0206	-0.0279	-0.0254	-0.0226	-0.0003
	0.0274	0.0408	0.0098	0.0103	0.0216	0.0258	0.0139	0.0080	0.0304	0.0302
NGC 4842A	-0.0788	0.0045	-0.0046	0.0248	0.0020	-0.0011	-0.0029	0.0553	-0.0260	-0.0109
	0.0305	0.0525	0.0144	0.0283	0.0116	0.0243	0.0342	0.0264	0.0268	0.0228
NGC 4864	-0.0463	-0.0213	-0.0332	-0.0201	-0.0546	-0.0346	-0.0846	-0.0345	-0.0176	-0.0735
	0.0220	0.0245	0.0128	0.0199	0.0217	0.0105	0.0401	0.0430	0.0143	0.0243
NGC 4865	-0.0038	-0.0181	-0.0227	0.0028	-0.0132	-0.0171	-0.0296	-0.0327	-0.0064	-0.0230
	0.0198	0.0113	0.0099	0.0116	0.0078	0.0050	0.0088	0.0158	0.0083	0.0144
NGC 4874	0.0337	-0.0280	-0.0413	-0.0550	-0.0234	-0.0151	-0.0366	-0.0511	-0.0290	0.0272
	0.0096	0.0122	0.0062	0.0146	0.0109	0.0078	0.0075	0.0104	0.0114	0.0154
NGC 4875	0.0087	-0.0172	-0.0451	-0.0163	-0.0050	-0.0055	-0.0165	0.0087	-0.0239	-0.0059
	0.0548	0.0173	0.0196	0.0745	0.0198	0.0241	0.0126	0.0221	0.0105	0.0291
NGC 4889	0.0087	-0.0246	-0.0385	-0.0031	-0.0303	-0.0603	-0.0505	0.0062	-0.0132	-0.0536
	0.0114	0.0075	0.0064	0.0061	0.0069	0.0058	0.0091	0.0123	0.0081	0.0128
NGC 4908	-0.0047	-0.0120	-0.0378	0.0004	0.0106	-0.0463	-0.0184	-0.0487	-0.0184	-0.0014
	0.0315	0.0322	0.0373	0.0152	0.0221	0.0104	0.0218	0.0274	0.0239	0.0381
NGC 5638	-0.0258	-0.0107	-0.0314	0.0013	-0.0135			-0.0357		
	0.0060	0.0052	0.0031	0.0056	0.0043			0.0064		
NGC 5796	-0.0004	-0.0172	-0.0235	-0.0011	-0.0110			-0.0328		
	0.0137	0.0096	0.0050	0.0066	0.0066			0.0100		
NGC 5812	-0.0177	-0.0249	-0.0338	-0.0003	-0.0272			-0.0265		
	0.0078	0.0060	0.0042	0.0062	0.0051			0.0076		
NGC 5813	-0.0179	-0.0119	-0.0168	0.0012	-0.0116			-0.0200		
	0.0063	0.0048	0.0044	0.0057	0.0040			0.0070		
NGC 5831	-0.0245	-0.0131	-0.0386	0.0053	-0.0154			-0.0365		
	0.0078	0.0069	0.0072	0.0063	0.0064			0.0059		
NGC 5845	-0.0161	-0.0150	-0.0293	0.0011	-0.0188			-0.0200		
	0.0091	0.0069	0.0085	0.0097	0.0059			0.0075		
NGC 5846	-0.0011	-0.0085	-0.0199	-0.0043	-0.0102	-0.0135	-0.0440	-0.0172	-0.0103	-0.0290
	0.0078	0.0047	0.0053	0.0069	0.0047	0.0038	0.0062	0.0064	0.0056	0.0059
NGC 5846A	-0.0246	-0.0161	-0.0468	-0.0093	-0.0009	-0.0227	-0.0714	-0.0499	-0.0151	-0.0308
	0.0125	0.0104	0.0079	0.0132	0.0158	0.0101	0.0066	0.0086	0.0070	0.0129
NGC 6127	-0.0072	-0.0079	-0.0374	-0.0059	-0.0227			-0.0217		
	0.0101	0.0073	0.0068	0.0074	0.0064			0.0202		
NGC 6166	-0.0207	-0.0208	-0.0271	0.0151	-0.0081	-0.0272	-0.0300	-0.0639	-0.0068	-0.0047
	0.0122	0.0132	0.0109	0.0076	0.0100	0.0066	0.0140	0.0163	0.0100	0.0152
NGC 6411	-0.0203	-0.0105	-0.0294	0.0023	-0.0101	-0.0200	-0.0274	-0.0176	-0.0040	-0.0150
	0.0074	0.0045	0.0055	0.0057	0.0054	0.0046	0.0042	0.0068	0.0052	0.0052
NGC 6482	-0.0249	-0.0143	-0.0190	0.0077	-0.0175	-0.0324	-0.0624	-0.0382	-0.0077	-0.0186
	0.0139	0.0117	0.0063	0.0088	0.0090	0.0061	0.0059	0.0084	0.0092	0.0109
NGC 6702	-0.0105	0.0039	-0.0325	-0.0174	-0.0219			-0.0058		
	0.0106	0.0089	0.0082	0.0075	0.0075			0.0188		

Table 1. continued.

Galaxia	Ca4455	Fe4531	C4668	H β	Fe5015	Mg ₁	Mg ₂	Mgb	Fe5270	Fe5335
NGC 6703	-0.0021	-0.0165	-0.0316	0.0025	-0.0160	-0.0152	-0.0399	-0.0245	-0.0122	-0.0157
	0.0061	0.0044	0.0034	0.0039	0.0036	0.0032	0.0040	0.0035	0.0039	0.0057
IC 832	0.0031	-0.0326	0.0040	0.0176	-0.0078	-0.0169	-0.0537	-0.0227	-0.0269	-0.0352
	0.0240	0.0216	0.0099	0.0142	0.0129	0.0150	0.0114	0.0142	0.0153	0.0178
IC 3957	-0.0385	0.0240	-0.0543	-0.0046	-0.0366	-0.0552	-0.0292	0.0003	-0.1654	-0.0976
	0.0067	0.0304	0.0164	0.0175	0.0378	0.0230	0.0185	0.0583	0.0726	0.0213
NGC 7052	-0.0109	-0.0038	-0.0193	0.0117	-0.0179	-0.0188	-0.0145	-0.0263	-0.0127	-0.0101
	0.0077	0.0071	0.0059	0.0064	0.0042	0.0037	0.0047	0.0056	0.0065	0.0069
NGC 7332	-0.0239	-0.0135	-0.0483	0.0118	-0.0028	-0.0506	-0.0646	-0.0215	-0.0195	-0.0197
	0.0055	0.0035	0.0042	0.0054	0.0064	0.0051	0.0113	0.0037	0.0043	0.0042
IC 767	0.0286	-0.0388	-0.0341	-0.0631	0.0389	0.1132	0.1299	0.0308	-0.0101	0.0096
	0.0073	0.0240	0.0358	0.0198	0.0232	0.0673	0.0540	0.0294	0.0221	0.0322
IC 794	0.0369	-0.0450	-0.0470	-0.0064	-0.0198			-0.0108		
	0.0216	0.0206	0.0146	0.0085	0.0110			0.0146		
IC 3959	-0.0097	0.0242	-0.0027	-0.0045	-0.0127	-0.0325	-0.0663	-0.0257	-0.0058	-0.0449
	0.0130	0.0287	0.0156	0.0112	0.0080	0.0090	0.0148	0.0141	0.0159	0.0169
IC 3963	0.0055	0.0022	-0.0462	-0.0131	-0.0149	-0.0302	-0.0312	-0.0289	-0.0155	-0.0204
	0.0236	0.0158	0.0105	0.0205	0.0119	0.0059	0.0097	0.0129	0.0124	0.0213
IC 3973	-0.0004	-0.0194	-0.0090	-0.0403	-0.0176	-0.0227	-0.0288	-0.0184	-0.0036	-0.0400
	0.0161	0.0291	0.0114	0.0318	0.0169	0.0117	0.0177	0.0271	0.0163	0.0161
IC 4042	-0.0124	-0.0252	-0.0516	0.0097	0.0174	0.0370	-0.0706	-0.0256	0.0603	-0.0823
	0.1930	0.0702	0.0385	0.0917	0.0554	0.0417	0.0617	0.0738	0.0338	0.0872
IC 4051	-0.0478	0.0055	-0.0500	0.0108	-0.0169	-0.0480	-0.0652	-0.0318	-0.0109	0.0066
	0.0153	0.0106	0.0128	0.0057	0.0087	0.0080	0.0097	0.0123	0.0131	0.0165
CGCG159-041	-0.0414	0.1280	0.0216	-0.0290	-0.0009	-0.0557	-0.1646	-0.1203	-0.1237	-0.0292
	0.0581	0.0502	0.0589	0.0668	0.1725	0.0105	0.0662	0.0453	0.0232	0.0269
CGCG159-043	-0.0389	-0.0126	-0.0285	-0.0389	-0.0307	-0.0343	-0.0590	-0.0318	-0.0202	-0.0390
	0.0152	0.0134	0.0213	0.0181	0.0161	0.0089	0.0128	0.0121	0.0108	0.0114
CGCG159-083	-0.0307	-0.0317	-0.0212	0.0527	-0.0084	-0.0165	-0.0213	-0.0334	-0.0009	-0.0249
	0.0192	0.0158	0.0131	0.0145	0.0169	0.0098	0.0148	0.0177	0.0139	0.0176
CGCG159-089	0.0046	0.0084	-0.0542	0.0231	-0.0331	-0.0371	-0.0617	-0.0271	-0.0121	-0.0188
	0.0333	0.0223	0.0071	0.0107	0.0158	0.0140	0.0103	0.0264	0.0124	0.0220

Table 2. Age and metallicity gradients derived with the method of Sect. 3 (second and third columns), and metallicity gradients derived in several index-index diagrams using different metallicity indicators (as indicated in the column headers) combined with H β . The second row for each galaxy indicates the associated errors in the gradients.

Galaxy	grad (age)	grad ([M/H])	CN ₂ grad ([M/H])	C4668 grad ([M/H])	Fe4383 grad ([M/H])	Mgb grad ([M/H])	Ca4227 grad ([M/H])
	$\pm\sigma$	$\pm\sigma$	$\pm\sigma$	$\pm\sigma$	$\pm\sigma$	$\pm\sigma$	$\pm\sigma$
NGC 221	0.0151	-0.0273	-0.170	-0.246	0.023	-0.171	0.082
	0.0180	0.0226	0.241	0.139	0.222	0.259	0.373
NGC 315	0.0850	-0.2745	0.010	-0.689	-0.214	-1.266	-0.209
	0.0486	0.0651	0.112	0.089	0.095	0.148	0.151
NGC 507	-0.6291	0.5756	0.076	0.451	1.004	0.453	0.935
	0.1508	0.2140	0.309	0.324	0.354	0.611	0.664
NGC 584	0.0814	-0.1937	-0.673	-0.510	-0.341	-0.414	-0.294
	0.0868	0.1185	0.196	0.114	0.145	0.242	0.355
NGC 636	0.0779	-0.3627	-0.740	-0.804	-0.427	-0.291	0.117
	0.1148	0.1592	0.220	0.200	0.300	0.274	0.382
NGC 821	0.0563	-0.8237	-1.560	-1.058	-0.493	-0.981	-1.057
	0.1157	0.9981	0.351	0.235	0.293	0.391	0.478
NGC 1453	-0.2652	-0.0141	-0.170	-0.246	0.023	-0.171	0.082
	0.1036	0.1259	0.241	0.139	0.222	0.259	0.373
NGC 1600	0.2293	-0.0732	-0.765	-0.521	-0.592	-0.561	-0.897
	0.0504	0.0708	0.116	0.072	0.121	0.216	0.203
NGC 1700	0.0803	-0.3432	-0.750	-0.693	-0.096	-0.384	0.534
	0.1116	0.1349	0.186	0.183	0.237	0.274	0.508
NGC 2300	0.1531	-0.2416	-0.553	-0.902	-0.335	-0.644	-0.049
	0.1284	0.1582	0.270	0.156	0.252	0.353	0.508
NGC 2329	0.2413	-0.3977	-0.610	-0.510	-1.081	1.243	-0.014
	0.1731	0.1840	0.346	0.284	0.377	0.884	0.478
NGC 2693	-0.1917	-0.0072	-0.420	-0.220	0.049	0.210	-0.168
	0.0786	0.0997	0.116	0.138	0.206	0.205	0.265
NGC 2694	-0.1551	-0.0214	0.119	-0.531	0.270	0.186	-0.882
	0.2540	0.2572	1.146	0.218	0.467	0.853	1.057
NGC 2778	0.0644	-0.3501	-1.041	-0.733	-0.284	-1.158	-0.233
	0.0879	0.1155	0.186	0.125	0.178	0.182	0.249
NGC 2832	0.1436	-0.3521	-0.819	-0.747	-0.712	4.801	-1.200
	0.0696	0.1046	0.120	0.102	0.196	1.205	0.297
NGC 3115	0.2518	-0.4864	-1.121	-0.691	-0.416	-0.692	-0.367
	0.0501	0.0845	0.154	0.070	0.090	0.103	0.129
NGC 3377	0.0334	-0.3600	-1.118	-0.960	-0.498	-1.143	-0.229
	0.0679	0.1147	0.152	0.103	0.241	0.214	0.222

Table 2. continued.

Galaxy	grad(log age) $\pm\sigma$	grad ([M/H]) $\pm\sigma$	CN ₂ grad ([M/H]) $\pm\sigma$	C4668 grad ([M/H]) $\pm\sigma$	Fe4383 grad ([M/H]) $\pm\sigma$	Mgb grad ([M/H]) $\pm\sigma$	Ca4227 grad ([M/H]) $\pm\sigma$
NGC 3379	0.1055	-0.2279	-0.515	-0.419	-0.239	-1.069	-0.262
	0.0347	0.0528	0.066	0.051	0.072	0.128	0.098
NGC 3605	0.0574	-0.3890	-0.050	-0.385	-0.869	-0.452	0.235
	0.1046	0.1486	0.218	0.191	0.278	0.288	0.348
NGC 3608	0.0595	-0.3767	-0.906	-0.575	-0.145	-0.706	0.104
	0.1043	0.1180	0.216	0.209	0.230	0.306	0.334
NGC 3641	0.0067	-0.3821	-1.608	-0.547	-0.209	-0.856	-0.261
	0.2529	0.2634	0.501	0.359	0.491	0.636	0.731
NGC 3665	0.0616	-0.1746	-0.092	-0.383	-0.105	-0.086	0.284
	0.0716	0.0941	0.166	0.095	0.163	0.215	0.285
NGC 3818	0.1865	-0.3875	-1.089	-0.874	-0.295	-0.840	-0.216
	0.0728	0.1087	0.152	0.106	0.147	0.172	0.203
NGC 4261	0.1011	-0.2411	-0.538	-0.350	-0.171	-0.335	-0.119
	0.0453	0.0597	0.075	0.068	0.091	0.132	0.184
NGC 4278	0.1895	-0.4505	-0.981	-0.623	-0.451	-1.034	-0.397
	0.0408	0.0647	0.081	0.056	0.095	0.121	0.132
NGC 4365	0.1087	-0.2385	-0.567	-0.459	-0.305	-0.586	-0.247
	0.0378	0.0542	0.069	0.050	0.077	0.091	0.121
NGC 4374	-0.1112	-0.0716	-0.452	-0.258	-0.000	-0.239	0.154
	0.0421	0.0668	0.109	0.077	0.092	0.126	0.158
NGC 4415	0.1048	-0.0759	0.074	-0.038	-0.071	-0.428	-0.581
	0.0625	0.0658	0.136	0.080	0.104	0.243	0.183
NGC 4431	0.1725	-0.1285	-0.610	-0.216	-0.260	-0.409	-0.548
	0.0928	0.1048	0.189	0.145	0.194	0.219	0.423
NGC 4464	-0.1041	-0.0150	-0.550	-0.206	-0.009	-0.374	0.213
	0.0796	0.0931	0.169	0.141	0.141	0.178	0.226
NGC 4467	0.0916	-0.5234	-0.798	-1.202	-0.719	-0.669	-0.303
	0.2661	0.2767	0.492	0.504	0.526	0.782	0.719
NGC 4472	0.1062	-0.3919	-0.543	-0.472	-0.220	-0.331	-0.506
	0.0252	0.0460	0.047	0.035	0.056	0.072	0.091
NGC 4478	0.1997	-0.2858	-0.508	-0.428	-0.391	-0.393	-0.454
	0.0508	0.0667	0.087	0.056	0.090	0.122	0.135
NGC 4486B	0.4092	-0.3663	-1.059	-0.891	-0.362	-1.184	-0.337
	0.2165	0.2441	0.260	0.200	0.483	0.442	0.576
NGC 4489	0.3077	-0.4354	-0.259	-0.700	-0.752	-0.359	-0.483
	0.1042	0.1423	0.228	0.164	0.260	0.228	0.492
NGC 4552	0.0526	-0.2075	-0.782	-0.584	-0.158	-0.546	-0.091
	0.0674	0.0939	0.127	0.076	0.151	0.144	0.287

Table 2. continued.

Galaxy	grad (age)	grad ([M/H])	CN ₂	C4668	Fe4383	Mgb	Ca4227
	$\pm\sigma$	$\pm\sigma$	grad ([M/H]) $\pm\sigma$	grad ([M/H]) $\pm\sigma$	grad ([M/H]) $\pm\sigma$	grad ([M/H]) $\pm\sigma$	grad ([M/H]) $\pm\sigma$
NGC 4564	0.1010	-0.3264	-0.842	-0.740	0.050	-0.520	-0.613
	0.0453	0.0635	0.107	0.059	0.080	0.109	0.131
NGC 4594	0.0938	-0.3880	-1.481	-0.929	-0.332	-1.162	-0.281
	0.1078	0.1491	0.272	0.142	0.335	0.353	0.496
NGC 4621	0.1645	-0.4335	-0.770	-0.702	-0.332	-0.594	-0.274
	0.0461	0.0718	0.097	0.067	0.114	0.143	0.184
NGC 4636	0.2275	-0.3357	-0.493	-0.446	-0.335	-0.768	-0.215
	0.0766	0.0981	0.178	0.120	0.158	0.182	0.289
NGC 4649	0.0305	-0.2151	-0.398	-0.465	-0.095	-0.364	-0.215
	0.0624	0.0845	0.159	0.105	0.142	0.137	0.261
NGC 4673	-0.1593	-0.1049	-0.231	-0.540	0.252	-0.580	-0.415
	0.0960	0.1239	0.176	0.175	0.213	0.249	0.339
NGC 4692	0.1630	-0.3817	-0.920	-0.737	-0.286	-0.802	-0.490
	0.1103	0.1285	0.233	0.204	0.251	0.305	0.349
NGC 4697	0.0425	-0.1537	-0.706	-0.502	-0.131	-0.403	-0.113
	0.0248	0.0423	0.046	0.040	0.055	0.071	0.086
NGC 4742	0.7591	-0.6467	-0.655	-0.771	-0.840	-1.174	-1.053
	0.0804	0.0949	0.129	0.098	0.143	0.182	0.207
NGC 4839	0.2800	-0.3535	-0.440	-0.460	-0.833	-0.898	0.056
	0.1708	0.1540	0.278	0.220	0.488	0.647	0.693
NGC 4842A	-0.2147	0.0637	-1.015	0.098	-0.324	1.459	1.735
	0.2617	0.2364	0.721	0.295	0.619	0.676	0.709
NGC 4864	0.4900	-0.5792	-0.479	-0.697	-1.175	-0.998	-0.692
	0.1762	0.1618	0.251	0.244	0.722	0.812	0.563
NGC 4865	0.0672	-0.2587	-0.410	-0.359	-0.143	-0.532	0.106
	0.1232	0.1416	0.370	0.175	0.261	0.339	0.368
NGC 4874	0.5845	-0.7181	-0.988	-1.078	-0.866	-1.955	-1.657
	0.1029	0.1382	0.225	0.136	0.265	0.316	0.411
NGC 4875	0.1777	-0.3231	-0.704	-0.869	-0.248	-0.152	-0.582
	0.1390	0.2141	0.852	0.588	1.212	1.398	1.876
NGC 4889	0.2578	-0.4363	-0.793	-0.665	-0.534	0.052	0.136
	0.0711	0.1120	0.182	0.109	0.163	0.237	0.307
NGC 4908	0.0131	-0.2354	-0.251	-0.629	-0.322	-0.864	0.613
	0.2231	0.2812	0.419	0.604	0.618	0.549	0.794
NGC 5638	0.0766	-0.3273	-0.774	-0.515	-0.140	-0.614	0.038
	0.0524	0.0673	0.097	0.061	0.103	0.147	0.187
NGC 5796	0.1234	-0.2664	-0.340	-0.400	-0.120	-0.608	-0.371
	0.0744	0.0938	0.133	0.091	0.148	0.208	0.216

Table 2. continued.

Galaxy	grad (age) $\pm\sigma$	grad ([M/H]) $\pm\sigma$	CN ₂ grad ([M/H]) $\pm\sigma$	C4668 grad ([M/H]) $\pm\sigma$	Fe4383 grad ([M/H]) $\pm\sigma$	Mgb grad ([M/H]) $\pm\sigma$	Ca4227 grad ([M/H]) $\pm\sigma$
NGC 5812	0.1436	-0.3077	-0.795	-0.567	-0.355	-0.480	-0.434
	0.0645	0.0881	0.117	0.079	0.127	0.172	0.214
NGC 5813	0.0150	-0.0826	-0.747	-0.272	-0.266	-0.335	-0.011
	0.0527	0.0634	0.105	0.078	0.113	0.156	0.202
NGC 5831	0.0299	-0.2412	-0.827	-0.608	-0.417	-0.553	-0.401
	0.0682	0.0980	0.127	0.123	0.142	0.149	0.230
NGC 5845	0.0536	-0.2156	-0.591	-0.482	-0.540	-0.337	-0.304
	0.1005	0.1117	0.244	0.150	0.180	0.216	0.287
NGC 5846	0.1258	-0.2327	-0.432	-0.363	-0.786	-0.389	0.369
	0.0554	0.0764	0.130	0.096	0.165	0.161	0.236
NGC 5846A	0.1829	-0.2979	-0.570	-0.848	-0.917	-1.069	-0.451
	0.1110	0.1620	0.265	0.156	0.305	0.278	0.488
NGC 6127	0.2307	-0.4596	-0.879	-0.667	-0.261	-0.500	-0.258
	0.0855	0.1293	0.240	0.118	0.179	0.375	0.344
NGC 6166	-0.1318	-0.0738	-0.131	-0.346	-0.284	-0.858	-0.329
	0.0920	0.1051	0.137	0.178	0.228	0.310	0.271
NGC 6411	0.0348	-0.1593	-0.477	-0.475	-0.255	-0.272	-0.166
	0.0528	0.0745	0.107	0.098	0.122	0.154	0.181
NGC 6482	0.0031	-0.1937	-0.472	-0.263	-0.214	-0.538	-0.318
	0.0877	0.0951	0.170	0.117	0.185	0.214	0.321
NGC 6702	0.3652	-0.5531	-0.522	-0.666	-0.353	-0.433	-0.168
	0.0854	0.1245	0.204	0.140	0.150	0.355	0.343
NGC 6703	0.0898	-0.2319	-0.526	-0.510	-0.186	-0.391	0.112
	0.0423	0.0684	0.102	0.059	0.089	0.093	0.132
NGC 7052	-0.0011	-0.1360	-0.215	-0.240	-0.018	-0.250	0.309
	0.0596	0.0763	0.112	0.105	0.123	0.153	0.196
NGC 7332	-0.0207	-0.0314	-0.698	-0.724	-0.180	-0.162	0.217
	0.0460	0.0768	0.096	0.075	0.110	0.113	0.157
IC 767	0.3838	-1.1858	-0.625	-1.015	-1.211	-0.642	-1.250
	0.1290	0.2090	0.459	0.579	1.359	0.619	0.683
IC 794	0.2383	-0.5238	-0.230	-0.831	-0.580	-0.314	0.112
	0.1220	0.1673	0.229	0.240	0.236	0.293	0.472
IC 832	-0.1432	0.0902	-0.329	0.191	0.242	-0.073	0.169
	0.1404	0.1483	0.291	0.182	0.330	0.351	0.710

Table 2. continued.

Galaxy	grad (age) $\pm\sigma$	grad ([M/H]) $\pm\sigma$	CN ₂ grad ([M/H]) $\pm\sigma$	C4668 grad ([M/H]) $\pm\sigma$	Fe4383 grad ([M/H]) $\pm\sigma$	Mgb grad ([M/H]) $\pm\sigma$	Ca4227 grad ([M/H]) $\pm\sigma$
IC 3957	0.2298	-0.4788	-0.890	-0.940	-0.202	-0.082	-2.087
	0.2385	0.2636	0.769	0.287	0.507	1.048	0.612
IC 3959	0.0731	-0.1642	-1.038	-0.077	0.091	-0.545	-0.565
	0.1344	0.1655	0.214	0.260	0.349	0.316	0.510
IC 3963	0.3360	-0.5703	-0.424	-0.864	-0.550	-0.765	-1.322
	0.1340	0.1788	0.300	0.217	0.387	0.436	0.595
IC 3973	0.4122	-0.3849	-0.692	-0.435	-0.532	-1.091	-0.595
	0.1776	0.1643	0.374	0.285	0.483	0.735	0.820
IC 4042	-0.1029	-0.3628	-0.161	-0.794	0.919	-0.275	0.785
	0.4661	0.6512	0.374	0.285	0.483	0.735	0.820
IC 4051	-0.0582	-0.3693	-0.873	-0.759	-0.224	-0.365	0.251
	0.0852	0.1261	0.165	0.208	0.184	0.234	0.411
CGCG 159-41	0.1629	-0.0679	-0.643	0.156	0.055	-2.702	0.558
	0.5742	0.6968	1.401	1.034	1.372	1.443	1.416
CGCG 159-43	0.5593	-0.6726	-0.902	-0.751	-0.480	-1.305	-0.820
	0.1614	0.1936	0.281	0.355	0.385	0.386	0.618
CGCG 159-83	-0.4099	0.0939	-0.902	-0.751	-0.480	-1.305	-0.820
	0.1310	0.1566	0.281	0.355	0.385	0.386	0.618
CGCG 159-89	-0.0815	-0.3979	-0.994	-0.743	0.570	-0.048	0.831
	0.1410	0.1969	0.229	0.134	0.351	0.484	0.513